1

2 **Title:** Hypoxia-inducible factor 1 signaling drives placental aging and can provoke preterm labor

3

4 **Authors**: Erin J. Ciampa[1], Padraich Flahardy[1], Harini Srinivasan[2], Christopher Jacobs[2], Linus Tsai[2],

5 S. Ananth Karumanchi[3], Samir M. Parikh[4]

6

7 **Affiliations**:

8 [1] Department of Anesthesia, Critical Care, and Pain Medicine, Beth Israel Deaconess Medical

9 Center, Harvard Medical School, Boston MA, USA

10 [2] Division of Endocrinology, Beth Israel Deaconess Medical Center, Harvard Medical School,

11 Boston MA, USA

12 [3] Department of Medicine, Cedars-Sinai Medical Center, Los Angeles CA, USA

13 [4] Division of Nephrology, Departments of Medicine and Pharmacology, University of Texas

14 Southwestern Medical School, Dallas TX, USA

15

16

17 Address correspondence to: Samir Parikh, MD. University of Texas Southwestern Medical

18 Center, Department of Internal Medicine. 5323 Harry Hines Blvd. Dallas, TX 75390-9030. Tel:

19 214-648-2754. Email: samir.parikh@utsouthwestern.edu.

20

Abstract:

Most cases of preterm labor have unknown cause, and the burden of preterm birth is immense. Placental aging has been proposed to promote labor onset, but specific mechanisms remain elusive. We report findings stemming from unbiased transcriptomic analysis of mouse placenta, which revealed that hypoxia-inducible factor 1 (HIF-1) stabilization is a hallmark of advanced gestational timepoints, accompanied by mitochondrial dysregulation and cellular senescence; we detected similar effects in aging human placenta. In parallel in primary mouse trophoblasts and human choriocarcinoma cells, we modeled HIF-1 induction and demonstrated resultant mitochondrial dysfunction and cellular senescence. Transcriptomic analysis revealed that HIF-1 stabilization recapitulated gene signatures observed in aged placenta. Further, conditioned media from trophoblasts following HIF-1 induction promoted contractility in immortalized uterine myocytes, suggesting a mechanism by which the aging placenta may drive the transition from uterine quiescence to contractility at the onset of labor. Finally, pharmacological induction of HIF-1 via intraperitoneal administration of dimethyloxalyl glycine (DMOG) to pregnant mice caused preterm labor. These results provide clear evidence for placental aging in normal pregnancy, and demonstrate how HIF-1 signaling in late gestation may be a causal determinant of the mitochondrial dysfunction and senescence observed within the trophoblast as well as a trigger for uterine contraction.

40 **Introduction:**

41 Preterm birth (birth prior to 37 completed weeks of gestation) is a massive global health
42 burden: it leads all causes of death in neonates and children to the age of 5 worldwide[1], and
43 survivors face a broad array of short- and long-term health challenges[2]. Most preterm births in
44 the United States are due to spontaneous onset of preterm labor, with unknown underlying
45 cause[3]. Preterm labor has proven difficult to treat; there currently exist no highly effective
46 interventions that prevent spontaneous preterm birth (SPTB)[4,5]. The dearth of effective
47 treatments stems from our lack of understanding about the pathways regulating spontaneous
48 onset of labor, both preterm and at term.

49

50 The placenta defines the maternal-fetal interface; it is capable of profoundly influencing both
51 maternal and fetal physiology[6-8], and it is subject to remodeling in response to its local
52 environment[9]. Placental disease is known to contribute to other disorders of pregnancy
53 including preeclampsia[10-12] and intrauterine growth restriction[13,14] and there is increasing
54 interest in its potential role as a driver of preterm labor[15-17].

55

56 Recent studies have found that placentas from pregnancies that resulted in SPTB have unique
57 metabolomic and transcriptomic signatures from term counterparts[18-20]. The reported
58 differences broadly implicate the stress response, inflammation, and various metabolic
59 pathways. It has been challenging to narrow these findings or translate them for mechanistic
60 relevance, given the lack of suitable culture systems that integrate experimental manipulation
61 of placental cells with the uterine myocyte response. Furthermore, interpretation studies

62 profiling human placentas from SPTB is sharply limited by the lack of gestational age-matched
63 controls. Without these, the effects of gestational age cannot be distinguished from factors
64 driving premature labor. The placenta encounters a dynamic local environment across its
65 lifetime and faces evolving needs of the growing fetus, so the context of normal gestational
66 age-related changes is vital for the correct interpretation of molecular characteristics
67 distinguishing a SPTB placenta. Defining the molecular-level changes in the *healthy* placenta as
68 it approaches the end of gestation, and their potential effects on the timing of labor onset
69 would therefore address important knowledge gaps.
70
71 Here we report findings from unbiased transcriptomic analysis of healthy mouse placenta,
72 which highlighted hypoxia-inducible factor 1 (HIF-1) signaling as a hallmark of advanced
73 gestational timepoints, accompanied by mitochondrial dysfunction and cellular senescence. We
74 detected some similar effects in human placentas, then modeled HIF-1 induction with two
75 different stimuli and in two trophoblast cell models, demonstrating that mitochondrial
76 dysfunction and cellular senescence arise secondary to HIF-1 stabilization. Whole transcriptome
77 analysis revealed that upon HIF-1 stabilization, a trophoblast cell line acquires signatures that
78 recapitulate the aged placenta. Finally, we show that conditioned media from these cells is
79 sufficient to potentiate a contractile phenotype in uterine myocytes, implicating a mechanism
80 by which the aging placenta may help drive the transition from uterine quiescence to
81 contractility at the onset of labor. This mechanism is further reinforced by an *in vivo* model in
82 which administration of the prolyl hydroxylase inhibitor dimethyloxalyl glycine (DMOG) to

83 pregnant mice induces HIF-1 signaling in the placenta and causes SPTB.

84

85 **Results**

86 To illuminate gestational age-dependent transcriptional changes in across a healthy pregnancy,
87 we collected whole mouse placentas at 48h intervals spanning embryonic day 13.5 to 17.5
88 (e13.5-e17.5) and quantified mRNA and protein targets that emerged from network analysis of
89 an independently published microarray dataset from healthy mouse pregnancies. Upon
90 searching Gene Expression Omnibus (GEO)[21] datasets for "placenta AND transcriptome", we
91 were surprised that among 326 results, only nine included data from normal placenta across a
92 series of gestational timepoints extending to late pregnancy[22-28] (**Figure 1**). We applied
93 weighted gene correlation network analysis (WGCNA) to a microarray study of mouse
94 placenta[22] (GEO accession GSE11224) spanning e8.5 to postnatal day 0 (p0) to assess the mRNA
95 signature of the aging mouse placenta, using the dataset with the best temporal resolution
96 across gestation. Distinct clusters emerged, each reflecting a group of genes whose expression
97 changes across timepoints in a unified way (**Figure 2A;** accompanying statistics available at
98 Mendeley Data, doi: 10.17632/g6vrw9jjn4.1). Genes in the 'blue' cluster showed increasingly
99 positive correlation with advancing gestational timepoints; KEGG functional pathways
100 significantly overrepresented among these genes include HIF-1 signaling, AMPK signaling, and
101 cellular senescence. Genes in the 'turquoise' cluster showed increasingly negative correlation to
102 advancing timepoints; KEGG functional pathways significantly overrepresented among these
103 genes include the citric acid cycle, mitochondrial complex I biogenesis, and the mitotic cell
104 cycle.

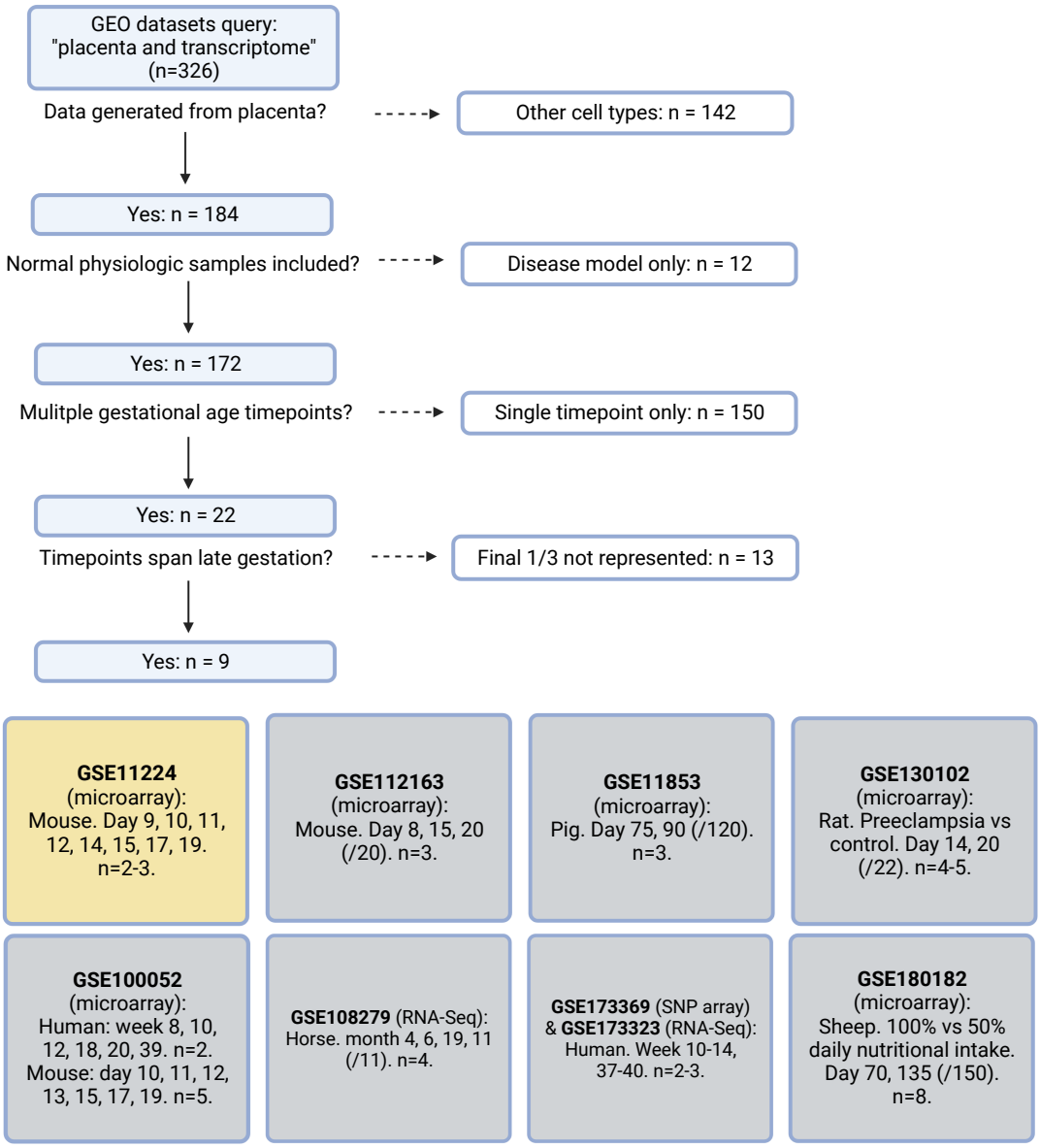

Figure 1. Systematic search flow for placental transcriptomics datasets. 326 GEO datasets were identified by the search terms "placenta" and "transcriptome"; nine met criteria for containing placental transcriptomic data representing normal physiology at a range of gestational timepoints spanning through the final 1/3 of pregnancy. Dataset selected for further analysis in yellow.

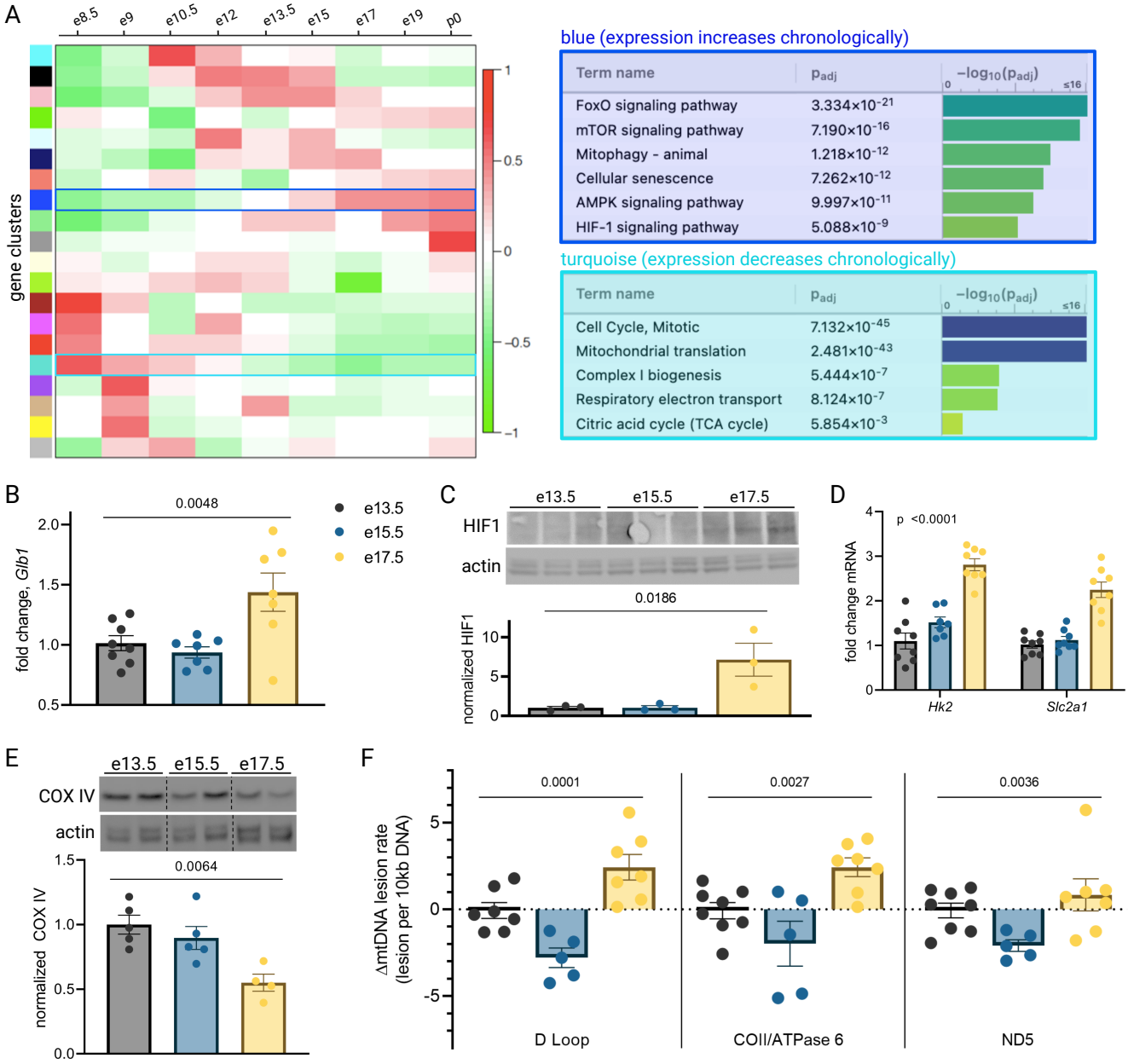

Figure 2. Mouse placental aging is characterized by cellular senescence, HIF-1 signaling, and mitochondrial dysregulation. WGCNA yielded 20 gene clusters. Functional pathways overrepresented in clusters found to increase (blue) and decrease (turquoise) across gestation highlight enhanced cellular senescence, increased HIF-1 signaling, and decreased mitochondrial synthesis and respiration late in pregnancy (A). mRNA expression of senescence marker *Glb1* peaks at e17.5 (B; one-way ANOVA p=0.0048). HIF-1 protein abundance is higher at e17.5 versus e13.5 and e15.5 (C; one-way ANOVA p=0.019), as is expression of HIF-1 targets *Hk2* and *Slc2a1* (D; two-way ANOVA p<0.0001 for gestational age factor). (See Figure 2 - Supplement 1 for analysis of gene expression changes across timepoints by placental sex.) Mitochondrial abundance, reflected by COX IV protein, decreases with gestational age (E, one-way ANOVA p=0.0064), and mitochondrial DNA lesion rate peaks at e17.5 in the regions of the D-loop (one-way ANOVA p=0.0001), COII/ATPase6 (p=0.0027), and ND5 (p=0.036) (F). B-F, Each data point represents a biological replicate (eg. RNA, protein, or DNA extracted from an individual placenta, in turn collected from one of 2-4 pregnant dams per group). Data normalized to mean at e13.5. See Figure 2 - Source Data 1 for uncropped blots.

105

106 To validate the dynamic pathway activity suggested by the WGCNA, we used qPCR to quantify
107 mRNA expression of the senescence marker *Glb1*[29] in our mouse placentas, which mirrored the
108 WGCNA finding that cellular senescence in the placenta peaks in the final days of gestation
109 (**Figure 2B**). HIF-1 protein abundance was found to peak at e17.5 (**Figure 2C**) and HIF-1 targets
110 *Hk2* and *Slc2a1* likewise confirmed increasing HIF-1 activation with advancing gestational age
111 through e17.5 (**Figure 2D**). Of note, a modest but significant fetal sex-dependent difference in
112 HIF-1 target expression (but not *Glb1*) was also observed across timepoints (**Figure 2 -**
113 **Supplement 1**). To assess changes in mitochondrial abundance across gestation, we measured
114 COX IV protein expression and found it declined progressively across mouse gestation (**Figure**
115 **2E**) as predicted by the WGCNA.

116

117 Having observed a pattern of declining mitochondrial abundance in the placenta with advancing
118 gestational age, we next investigated the mitochondrial DNA (mtDNA) lesion rate. The
119 mitochondrial genome is particularly vulnerable to reactive oxygen species (ROS) insults, and
120 mtDNA damage participates in a vicious cycle with mitochondrial dysfunction and further ROS
121 production; these effects are observed in a number of age-related diseases in various tissues[30]
122 and may drive age-associated loss of function[31]. We employed a semi-long run real-time qPCR
123 approach[32] to quantify relative mtDNA lesion rates in mouse placentas, normalized to e13.5.
124 There was a measurable increase in the mtDNA lesion rate in the D-loop and COII/ATPase 6
125 regions of the mitochondrial genome at e17.5 (**Figure 2F**). Together, these results reflect a
126 series of coordinated changes as gestation progresses —namely HIF-1 signaling induction,

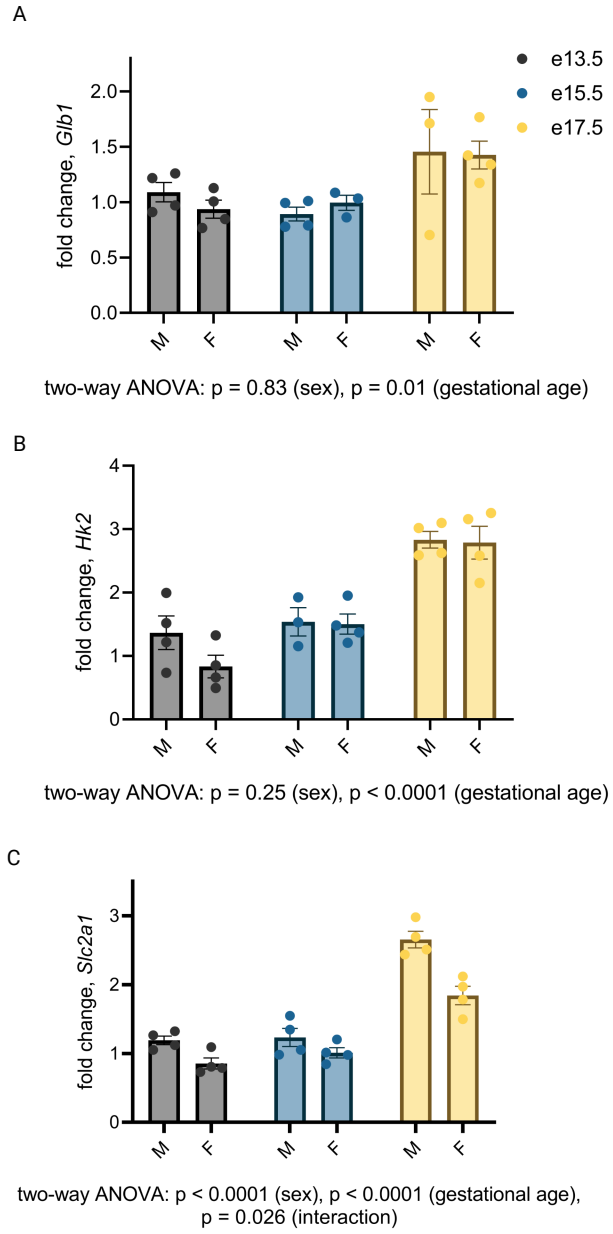

Figure 2 - Supplement 1. Gestational age-dependent variability in expression of Hif-1 target *Slc2a1*, but not *Hk2*, is affected by placental sex. Subgroup analysis did not reveal sex-dependent mRNA expression changes in *Glb1* (A) or *Hk2* (B) by qPCR, but did demonstrate consistently higher *Slc2a1* expression in male placentas at all gestational ages and an interaction between the effects of sex and gestational age on *Slc2a1* expression (C; two-way ANOVA p<0.0001 for sex, p<0.0001 for gestational age, and p=0.028 for interaction). Each data point represents a biological replicate (RNA isolated from an individual placenta, collected from one of 2-4 dams per group). Data normalized to collective (M+F) mean at e13.5.

127 decreasing mitochondrial abundance, accumulating mtDNA damage, and escalating cellular
128 senescence — confirming the patterns we discovered through reanalysis of published
129 transcriptomic data.
130
131 We next probed human placentas for the same gestational age-dependent changes. Studying
132 normal human placenta at a range of gestational ages beyond the second trimester is
133 challenging, as placental sampling is usually only possible after delivery, and most deliveries
134 associated with healthy pregnancies occur at term. We therefore sought to capitalize on rare
135 exceptions such as cases of placenta previa, vasa previa, or uterine dehiscence, where
136 iatrogenic preterm delivery is indicated for reasons unrelated to placental health. With an
137 objective to compare term versus preterm placentas, yet minimize confounding factors that
138 accompany labor and disease states that could be expected to affect placental health, we
139 designed a case-control study using the following exclusion criteria: onset of labor prior to
140 delivery (spontaneous or induced); maternal history of hypertension, asthma, diabetes, or
141 autoimmune disease; pregnancy complicated by gestational hypertension, gestational diabetes,
142 preeclampsia, multiples, fetal anomalies, placenta accreta spectrum disorder, or smoking
143 during pregnancy.
144
145 Placentas from 9 cesarean deliveries occurring before 35 weeks gestation and 11 cesarean
146 deliveries occurring after 39 weeks gestation were studied (**Table 1**). Maternal characteristics
147 including race, nulliparity, and obesity were not statistically different across the early versus
148 late groups; there was a small but statistically significant difference in maternal age at the time

149 of delivery (31.9 ± 0.9 years versus 36.2 ± 1.0 for early gestation versus late, p = 0.008). The
150 distribution of fetal sex was not different among groups.
151
152 qPCR revealed a trend toward increased mRNA expression of *GLB1* and HIF-1 targets *HK2* and
153 *SLC2A1* in the > 39-week cohort (**Figure 3A**), consistent with the gestational age-dependent
154 effect seen in mouse placenta. We also examined mitochondrial abundance in the two groups
155 and found that mitochondrial RNA transcripts *ATP6* and *COX2* were significantly decreased
156 (**Figure 3B**) and COX IV protein abundance was lower at the later timepoint (**Figure 3C**),
157 mirroring the mouse findings. Of note, power calculation to reject the null hypothesis for
158 difference between means for some of these measurements (with α=0.05 and β=0.2) suggests
159 a sample size of greater than 35 per group is required, assuming a similar effect size as seen in
160 mouse data (eg. expecting *GLB1* fold change difference of 40% across groups), and greater
161 variability than seen for mouse data (eg. expected standard deviation of *GLB1* fold change
162 equal to 0.6, versus 0.3 in mice). Practical constraints, especially given our strict exclusion
163 criteria, make a study of this size unfeasible; nonetheless, we have included analysis of 20
164 human placentas here in recognition of the vital importance of translating mouse findings to
165 human biology, even preliminarily. The data should be interpreted in the context of these
166 statistical realities.
167
168 The co-appearance of cellular senescence, HIF-1 signaling, and mitochondrial dysregulation in
169 the placenta as it approaches the end of gestation led us to hypothesize that in aging placental
170 cells, HIF-1 induction could be upstream of mitochondrial dysregulation and cellular

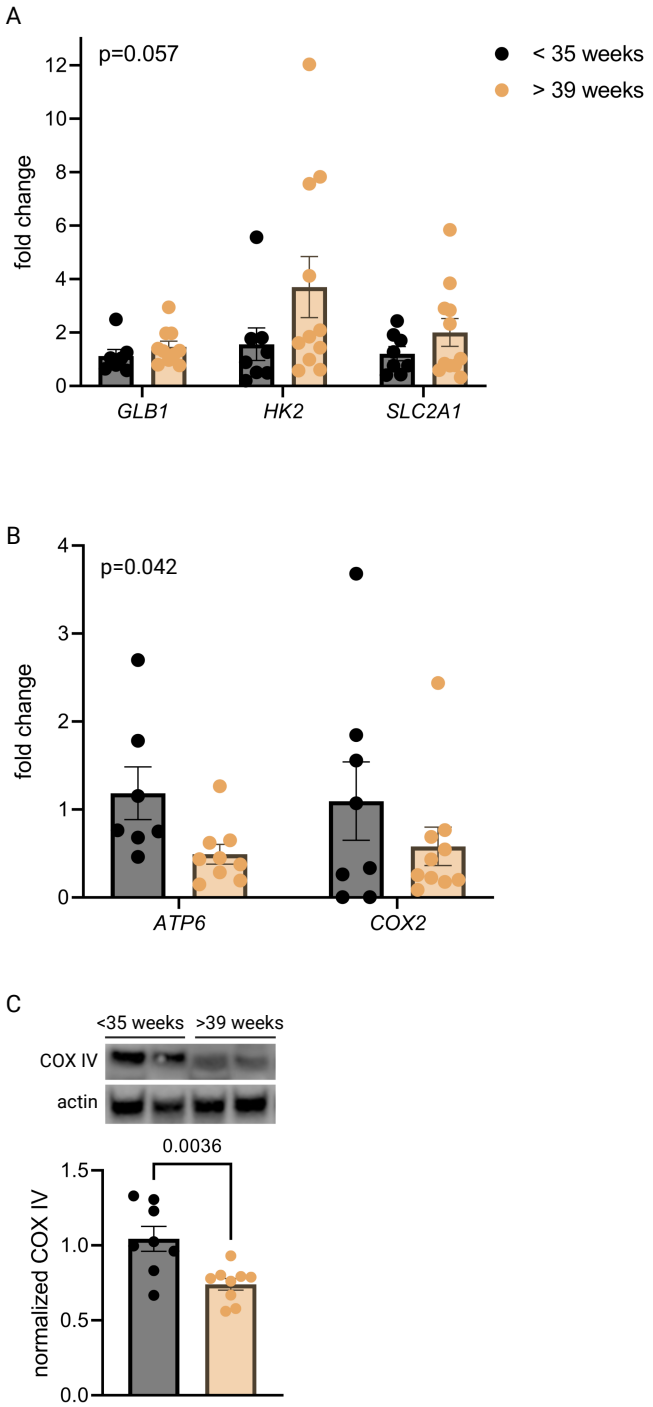

Figure 3. Senescence, HIF-1 signaling, and decreased mitochondrial abundance characterize late-gestation human placenta. mRNA expression of senescence marker *GLB1* and HIF-1 targets *HK2* and *SLC2A1* trends higher in placentas from > 39-week cohort vs < 35-week cohort (A; 2-way ANOVA gestational age factor p=0.057). Mitochondrial abundance, reflected by mitochondrial genes *ATP6* and *COX2* (B; two-way ANOVA gestational age factor p=0.042) and COX IV protein (C; p=0.0036) decreases with advancing gestational age. Each data point represents a biological replicate (RNA or protein isolated from an individual placenta). Data normalized to mean in < 35 week group. See Figure 3 - Source Data 1 for uncropped blots.

171 senescence, as is seen in other systems in emerging aging research[33-35]. To test this hypothesis,
172 we established a pharmacological model of HIF-1 induction in primary mouse trophoblasts
173 using cobalt chloride, a prolyl hydroxylase inhibitor that stabilizes HIF-1α[36,37] and has been
174 widely used to model hypoxia. After six hours of $CoCl_2$ exposure, we confirmed HIF-1 protein
175 accumulation in cultured trophoblasts (**Figure 4A**). After 48 hours of $CoCl_2$ exposure, mouse
176 trophoblasts exhibit decreased mitochondrial abundance, by *Cox2* mRNA expression (**Figure 4B**)
177 and Cox IV protein abundance (**Figure 4C**), and an increase in senescence-associated beta
178 galactosidase (SA-βGal), encoded by *Glb1* (**Figure 4D**) and detected as a blue stain in an X-gal
179 assay for senescence (**Figure 4E**). These findings suggest that HIF-1 stabilization induces
180 subsequent mitochondrial dysfunction and senescence in trophoblasts.
181
182 Primary trophoblasts undergo spontaneous syncytialization in culture, a phenomenon that
183 limits the duration of study and may also confound the interpretation of experimental changes
184 in key metabolic factors[38]. We therefore also modeled HIF-1 activation in JAR cells, a
185 trophoblast cell line that does not undergo syncytialization[39]. Consistent with our results in
186 primary cells, we found that HIF-1 is stabilized in $CoCl_2$-treated JAR cells (**Figure 5A**), and after 6
187 days of exposure, mitochondrial DNA and protein abundance declined (**Figure 5B-C**). We
188 further defined the time course of mitochondrial downregulation: by 72 hours the effect began
189 to appear (**Figure 5 – Supplement 1**). Furthermore, at the 6-day timepoint we found that $CoCl_2$
190 exposure leads to accumulation of mitochondrial ROS, as measured by mtSOX, a fluorescent
191 mt-superoxide indicator dye (**Figure 5D**), and impairs mitochondrial polarization, as measured
192 by tetramethylrhodamine ethyl ester (TMRE) staining, a cell-permeant fluorescent dye that

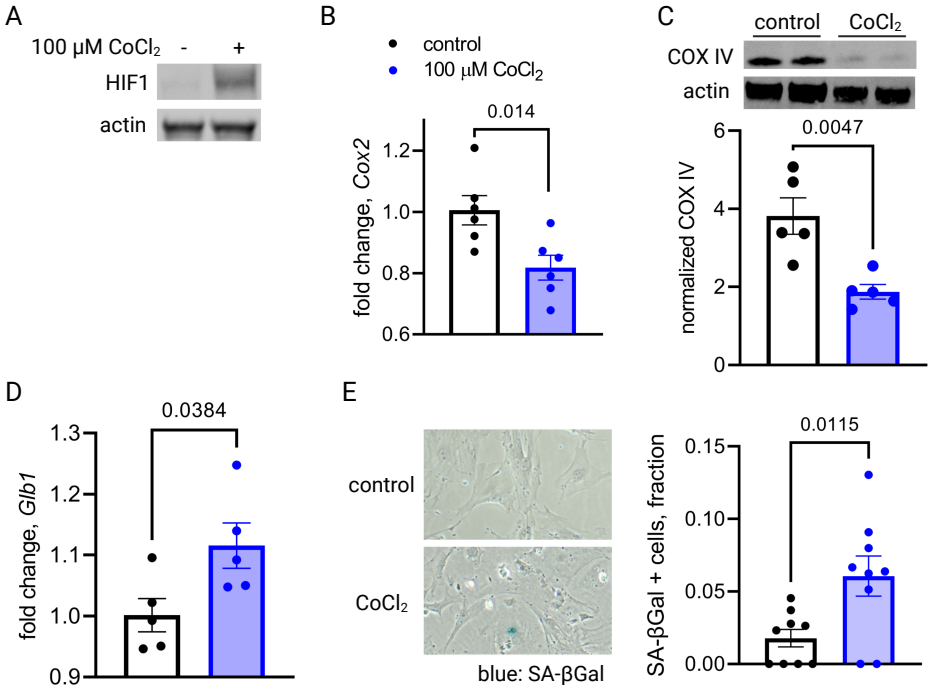

Figure 4. Short-term HIF-1 stabilization in primary mouse trophoblasts leads to decreased mitochondrial abundance and cellular senescence. HIF-1 is detected in cultured trophoblasts exposed to $CoCl_2$ (A). After 48 hours of $CoCl_2$ exposure, trophoblasts exhibit decreased mitochondrial abundance reflected by *Cox2* mRNA expression levels (B; p=0.014) and COX IV protein levels (C; p=0.0047). Senescence marker *Glb1* is increased (D; p=0.038) and SA-βGal accumulation is noted by X-gal assay (E; p=0.012). Each data point represents a technical replicate (eg. protein, RNA, or β-Gal measured from an individual well of cells grown in treated or control condition). Data normalized to mean of control treatment group. See Figure 4 - Source Data 1 for uncropped blots.

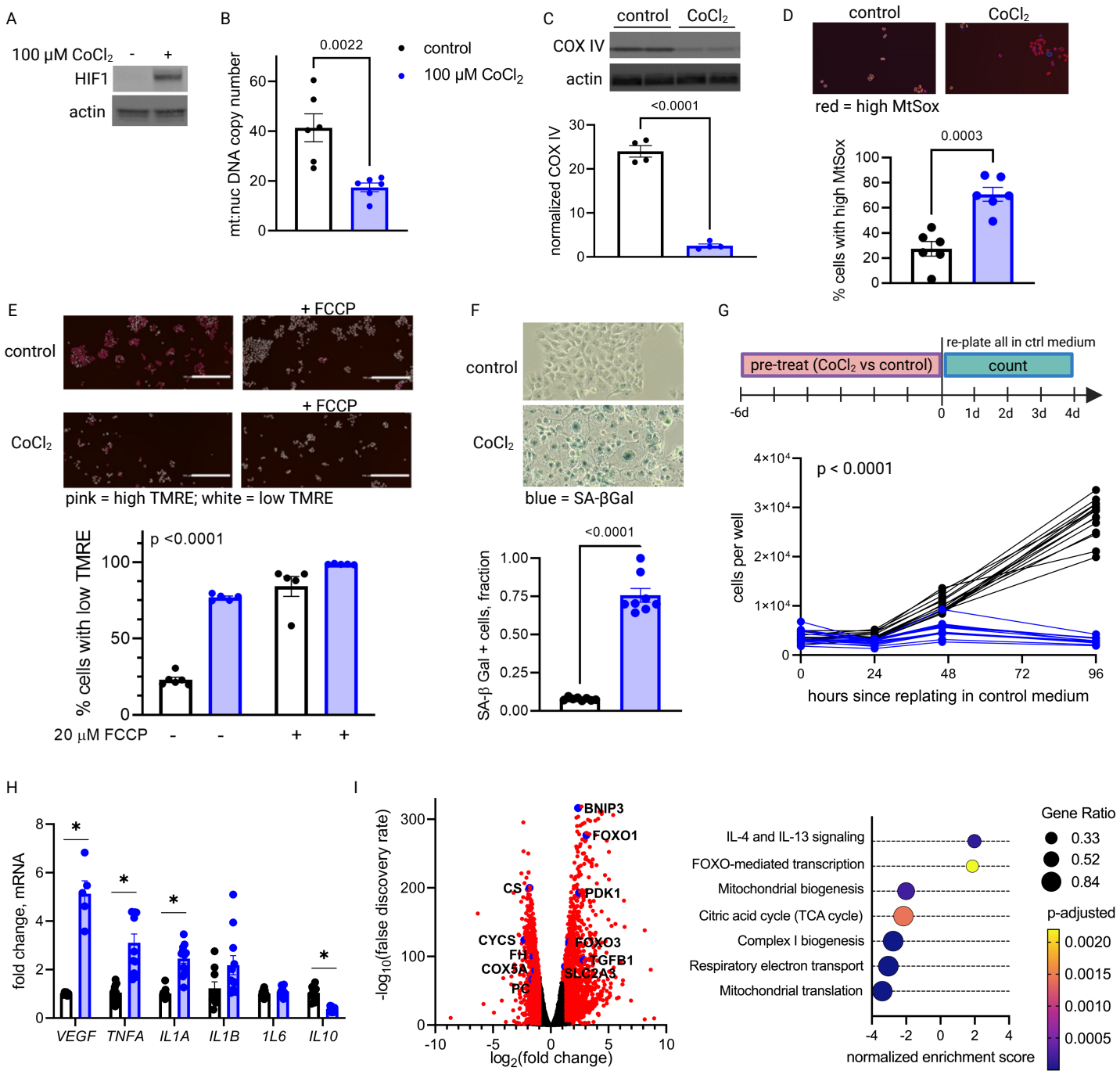

Figure 5. Long-term HIF-1 stabilization in JAR cells leads to mitochondrial dysfunction, cellular senescence, and metabolic reprogramming. HIF-1 is stabilized at 6 day timepoint of $CoCl_2$ exposure (A). After 6 days, mitochondrial abundance is decreased as reflected by a drop in the mitochondrial:nuclear DNA copy number (B) and a decrease in COX IV protein (C). (See Figure 5 - Supplement 1 for timecourse of declining mitochondrial abundance.) Cells also exhibit augmented signs of mitochondrial dysfunction via MtSox (D; p=0.0003) and TMRE staining (E; two-way ANOVA $CoCl_2$ factor p<0.0001). SA-βGal staining reflects a high proportion of senescent cells (F; p<0.0001) and growth arrest is confirmed by cell counting following a 6-day pre-treatment with $CoCl_2$ (G; two-way ANOVA p<0.0001 for interaction of $CoCl_2$ factor with time). (See Figure 5 - Supplement 2 for assessment of cell death by propidium iodide staining.) mRNA expression of SASP candidates *VEGF*, *TNFA*, *IL1A*, and *IL10* is altered after $CoCl_2$ exposure (H; *, adjusted p<0.01). RNA Seq revealed upregulation of 2188 and downregulation of 1389 genes (I; genes with $|\log_2(FC)| > 1$ and -log(FDR)>2 indicated in red) after $CoCl_2$ treatment, with geneset enrichment analysis revealing several pathways significantly dysregulated after $CoCl_2$ treatment recapitulating changes seen in transcriptomic analysis of late versus early gestation mouse placenta. Scale marker = 200 μm. FCCP= carbonyl cyanide 4-(trifluoromethoxy) phenylhydrazone, an ionophore uncoupler of oxidative phosphorylation which depolarizes mt membrane potential. See Figure 5 - Supplement 3 for assessment of effects of HIF-1 stabilization in JAR cells using DMOG. Each data point represents a technical replicate (measurement from an independent well of cells grown in treatment vs control condition). Data normalized to mean of control group. See Fig 5 Source Data 1 for uncropped blots.

193 accumulates in polarized mitochondria (**Figure 5E**). Additionally, we observed pronounced signs
194 of cellular senescence: morphological hallmarks (cellular swelling) and β-galactosidase
195 overexpression (**Figure 5F**); growth arrest which persists for days after removal of the HIF-1
196 stabilizing compound (**Figure 5G**); and a senescence-associated secretory phenotype (SASP,
197 **Figure 5H**) reflected by increases in mRNA expression of the genes encoding VEGF, TNFα and IL-
198 1α and a decrease in mRNA expression of the gene encoding anti-inflammatory cytokine IL-10.
199
200 We conducted additional studies to confirm that cell death was not a primary contributor to
201 the lack of proliferation. Propidium iodide staining with quantitative fluorescence cytometry
202 indicated that $CoCl_2$ treatment only increased cell death by 0-3% (**Figure 5 - Supplement 2**).
203 Importantly, cells remained adherent and continued to acidify culture medium beyond 14 days
204 of $CoCl_2$ exposure, providing confidence that HIF-1 stabilization induces a phenotype
205 characterized by predominantly viable cells that are no longer proliferating, namely cellular
206 senescence. Finally, to assess whether the effects we observed were attributable to HIF-1
207 stabilization and not an off-target effect of $CoCl_2$, we also evaluated an alternative prolyl
208 hydroxylase inhibitor, dimethyloxalylglycine (DMOG)[40], and found similar effects on HIF-1,
209 mitochondrial abundance and cellular senescence (**Figure 5 – Supplement 3**).
210
211 To determine if other features of the aged placenta phenotype were recapitulated in this
212 model, we performed whole transcriptome analysis via RNA-Seq. Differential expression ($\log_2$
213 fold change > 1; FDR < 0.05) was found for 2188 upregulated and 1389 downregulated genes
214 (**Figure 5I**). Gene set enrichment analysis revealed that chemical hypoxia led to upregulation of

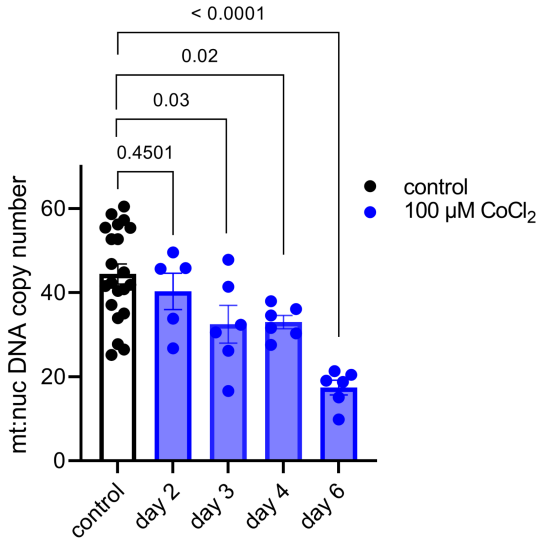

Figure 5 - Supplement 1. The mitochondrial effects of HIF-1 stabilization in JAR cells begin to appear on day 3 following $CoCl_2$ exposure. Each data point represents a technical replicate (independent well of cells grown in control vs treatment condition).

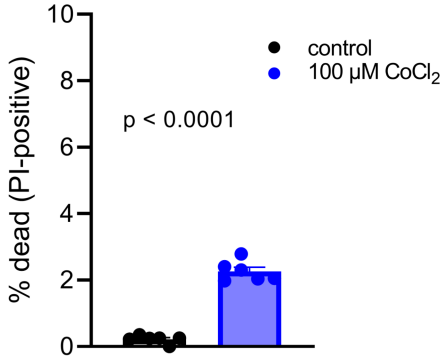

Figure 5 - Supplement 2. Increased number of JAR cells stain with propidium iodide, but the absolute number remains low following 6 days of $CoCl_2$ treatment. Each data point represents a technical replicate (independent well of cells grown in control vs treatment condition).

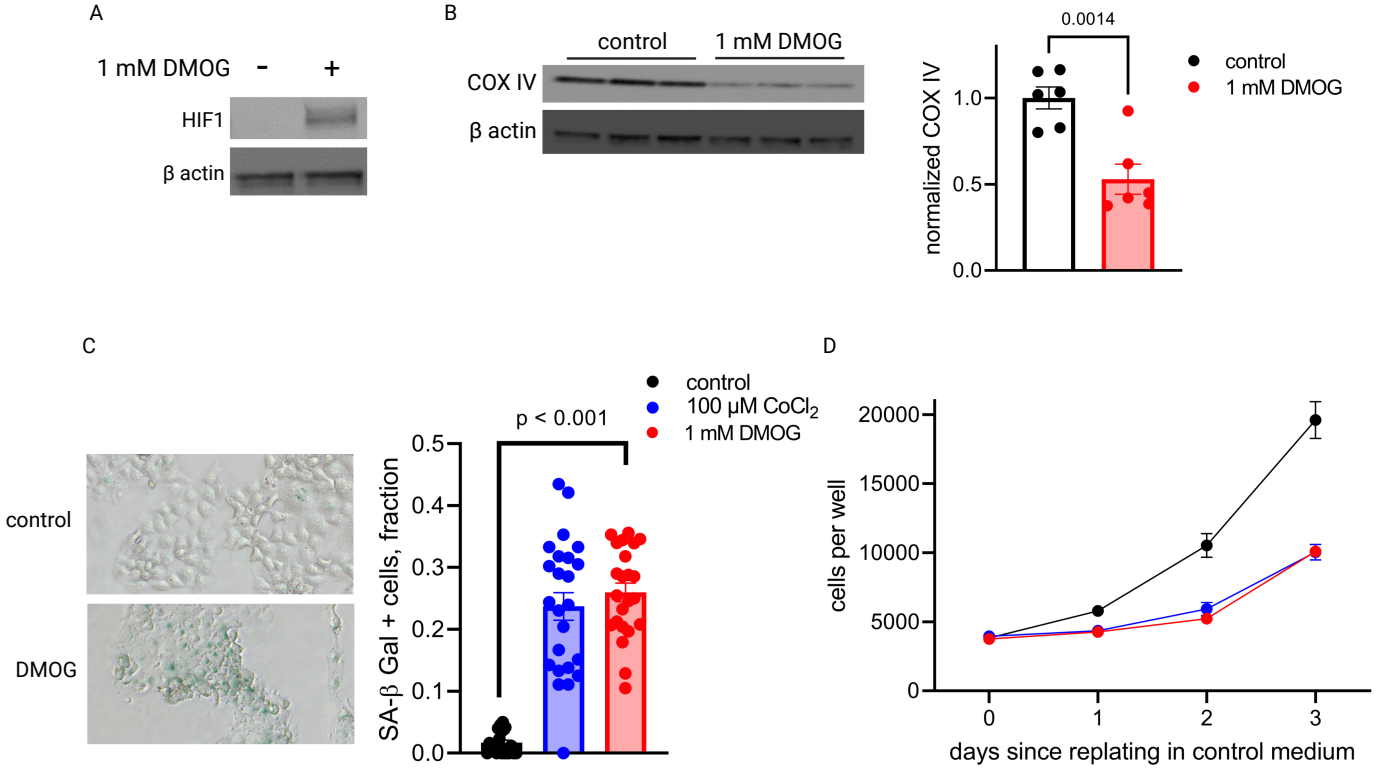

Figure 5 - Supplement 3. DMOG stabilizes HIF-1 in JAR cells (A) and induces similar effects as $CoCl_2$ on COX IV protein (B), SA-βGal expression (C), and cell growth (D) after 4 days. Each data point represents a technical replicate (measurement from an independent well of cells grown in treatment vs control condition). See Figure 5 - Source Data 1 for uncropped blots.

215 inflammatory signaling, and downregulation of the TCA cycle, mitochondrial biogenesis, and
216 respiratory electron transport. These data therefore recapitulated metabolic patterns that
217 emerged from time course transcriptomic analysis of intact placentas (Figure 2A).
218
219 The onset of labor is accompanied by a transformation of the uterus from quiescence into a
220 distinct physiologic state in which it generates powerful, coordinated contractions. This
221 phenotypic change is characterized by upregulation of a cadre of contraction associated
222 proteins (CAPs), notably: cyclooxygenase-2 (COX-2, encoded by *PTGS2*), prostaglandin F2α
223 receptor (encoded by *PTGFR*), interleukin-6 (IL-6), and connexin 43 (Cx43, encoded by *GJA1*)
224 Phenotypic switching can be modeled in primary and immortalized uterine myocytes upon
225 stimulation with inflammatory mediators such as IL-1β, PGF2α, and thrombin[41-43].
226
227 To test whether primary placental metabolic disruptions could crosstalk with uterine myocytes
228 to trigger the contractile phenotype, we collected conditioned media from our JAR cell model
229 of HIF-1-driven senescence and measured the effect on expression of CAPs in uterine myocytes
230 (hTERT-HM cells). We observed a robust and specific effect: co-stimulation of uterine myocytes
231 with IL-1β plus conditioned media from JAR cells treated with $CoCl_2$ (but not from untreated
232 JAR cells) potentiated the induction of *PTGS2*, *GJA1*, *PTGFR*, and *IL6* mRNA expression (**Figure**
233 **6A-D**). We next employed a collagen lattice assay previously described for assessing
234 contractility of myometrial cells *in vitro*[41,44], and demonstrated that myocyte contraction is
235 augmented upon exposure to conditioned media from JAR cells treated with $CoCl_2$ but not from
236 untreated JAR cells (**Figure 6E**). These transcriptional and functional results collectively

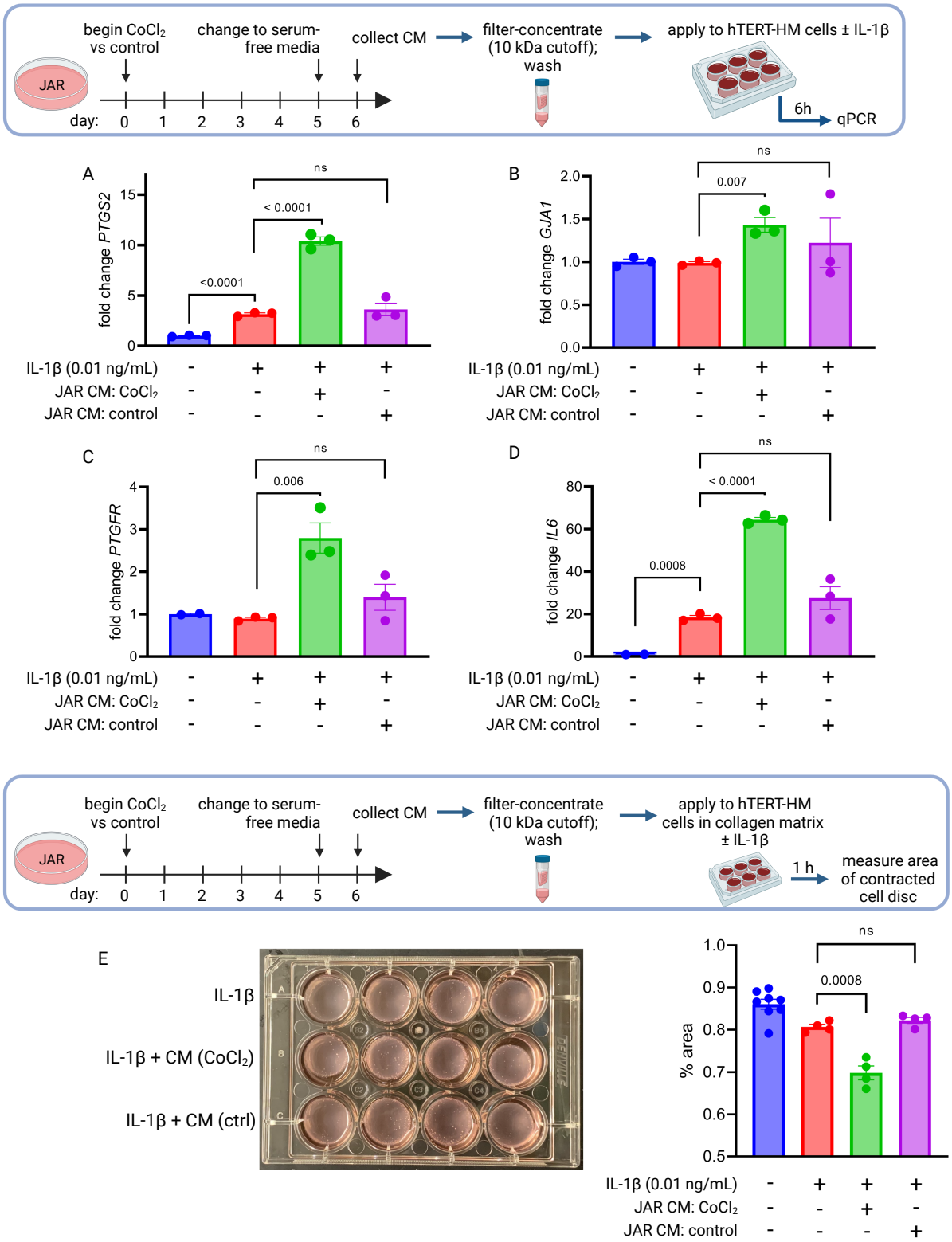

Figure 6. Conditioned media (CM) from JAR cells following HIF-1 stabilization induces expression of contractile-associated proteins and augments contraction in immortalized human uterine myocytes. hTERT-HM mRNA expression of *PTGS2* (A), *GJA1* (B), *PTGFR* (C), and *IL6* (D) was induced by CM from JAR cells following $CoCl_2$ treatment (but not in control conditions), potentiating the effect of stimulation of myocytes by exogenous IL-1β. Data normalized to mean of null treatment group. Percent well area occupied by hTERT-HM cells embedded in collagen matrix is significantly smaller after stimulation with IL-1β plus JAR CM from $CoCl_2$ condition, reflecting greater degree of hTERT-HM cellular contraction (E). Each data point represents a technical replicate (measurement from an independent well of cells grown in treatment vs control condition).

237 demonstrate that uterine myocytes are responsive to the secretome of JAR cells driven to
238 senescence via HIF-1 induction.
239
240 To test whether HIF-1 induction drives labor onset *in vivo*, we administered DMOG
241 intraperitoneally to pregnant mice on gestational day e16.5. Analysis of placentas recovered 12
242 hours following injection indicated that HIF-1 protein is stabilized in placenta following
243 maternal DMOG injection (**Figure 7A**), and transcription of HIF-1 target genes *Hk2* and *Slc2a1*
244 was significantly increased (**Figure 7B**). Following injection of DMOG, gestational length was
245 significantly shortened compared to injection of vehicle alone (**Figure 7C-D**).
246
247 **Discussion**
248 The subject of whether the healthy placenta undergoes aging (with accompanying dysfunction)
249 within its 40-week lifespan has been of great interest and debate for many years. Age-related
250 functional decline is a near-universal phenomenon affecting many tissues, but the underlying
251 biochemical driving factors vary widely depending on the context of cell type and local
252 stressors. Mechanisms well described in other tissues are rooted in genomic instability,
253 mitochondrial dysfunction and oxidative stress, nutrient deprivation and metabolic
254 insufficiency, or loss of proteostasis[45]. While characterization of the placenta as an aging organ
255 appeared in the literature beginning nearly fifty years ago[46,47], a counter-argument has been
256 offered that there is no logical reason for the placenta to undergo accelerated aging relative to
257 the fetus, since both share the same genes and environment[48]. A third viewpoint proposes that
258 aging in the placenta is indicative of a disease state—not normal progression of healthy

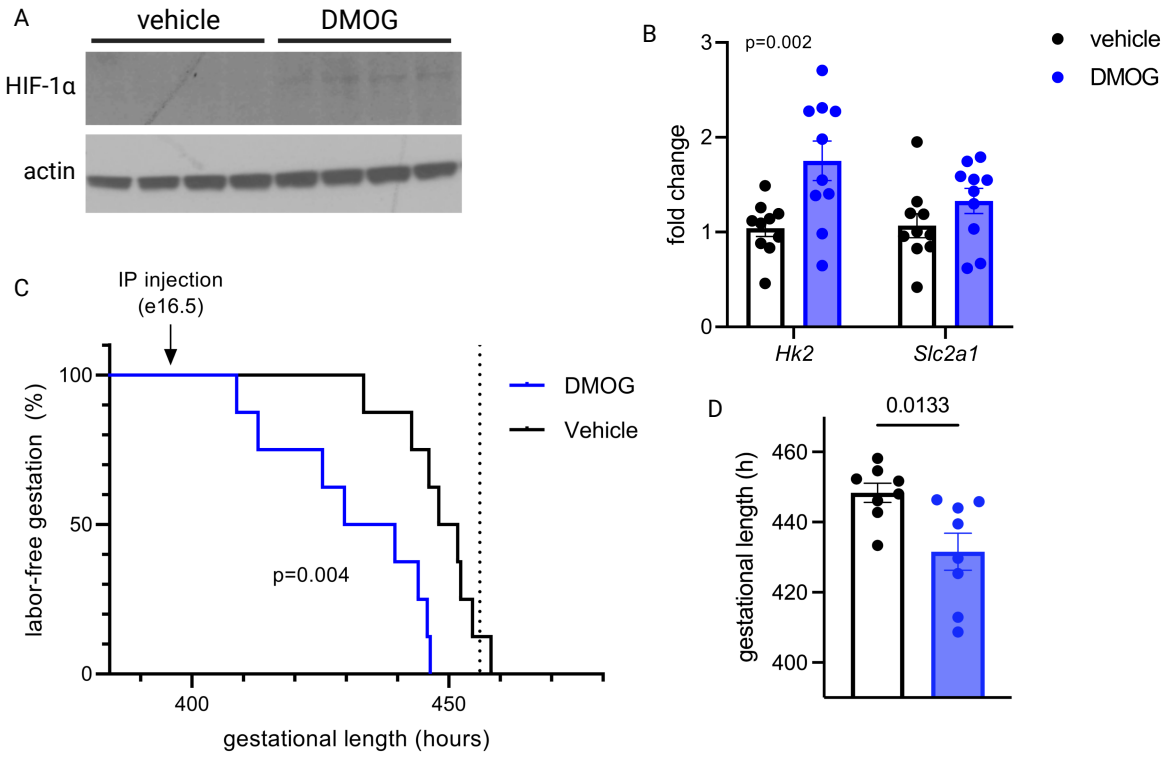

Figure 7. Maternal DMOG injection on e16.5 stabilizes placental HIF-1 and induces preterm labor. HIF-1α protein is detected in placental lysates 12 hours following DMOG injection but not vehicle (A). mRNA expression of HIF-1 targets *Hk2* and *Slc2a1* is upregulated following DMOG injection (p = 0.002 for DMOG vs vehicle, two-way ANOVA) (B). Gestational length is significantly shortened following DMOG injection versus vehicle (C-D). Each data point represents a biological replicate (in A and B, each measurement from an individual placenta collected from one of 2 pregnant dams). Data normalized to mean of vehicle group. See Figure 7 - Source Data 1 for uncropped blots.

259 gestation—one usually reflective of maladaptive responses to oxidative stress[49-53]. Finally,
260 recent reports have noted prominent signs of aging in another fetally derived tissue, the
261 chorioamniotic membranes, in healthy pregnancies[54], and have linked aging of the fetal
262 membranes to the onset of labor[55,56]. The results presented here span mouse and human
263 placentas to provide evidence for placental aging in normal pregnancy. Mechanistic dissection
264 of this phenomenon further demonstrates how hypoxia in late gestation may be both a causal
265 determinant of mitochondrial dysfunction and senescence observed within the trophoblast as
266 well as a trigger to induce uterine contraction.
267
268 To our knowledge, this is the first report to propose that placental aging in healthy pregnancy is
269 characterized by induction of HIF-1 signaling, accompanied by downstream effects including
270 mitochondrial dysfunction and cellular senescence. These findings have implications for the role
271 of the placenta in signaling that promotes the onset of labor, particularly given our
272 demonstration that upon HIF-1 stabilization, trophoblasts can induce inflammatory changes in
273 uterine myocytes and potentiate their contractility, and our *in vivo* demonstration that
274 administration of DMOG stabilizes placental HIF-1 and leads to preterm labor in mice.
275 Important next steps prompted by this work include determining the specific components of
276 the secretome of HIF-1-activated trophoblasts which are responsible for inducing myocyte
277 transformation, anticipating overlap with findings of prior studies delineating paracrine signals
278 that mediate labor onset[57-60]. Additionally, having established that HIF-1 signaling is upstream
279 of mitochondrial dysfunction and cellular senescence in late-gestation placenta in normal
280 pregnancies, future studies can investigate whether factors that modulate this pathway could

281 increase or decrease vulnerability to preterm labor. In studies targeted to uterine decidua, a
282 link between cellular senescence and labor onset has previously been established, with
283 evidence implicating phospho-Akt and mTORC1 signaling upstream of prostaglandin synthesis
284 as a key mechanism in this model[61,62]. It is possible that senescence signaling from the placenta
285 and decidua converge, and labor is provoked upon these convergent endpoint signals
286 surpassing a threshold, regardless of their origin within the gestational compartment. Future
287 studies using targeted manipulation of senescence and metabolism in these compartments
288 individually will help clarify their specific contributions to labor onset.
289
290 Our results suggest that placental HIF-1 becomes stabilized late in gestation, and this could be
291 secondary to the onset of hypoxia sensing as oxygen demand outstrips supply in the
292 fetoplacental unit. However, placental hypoxia has been difficult to examine *in vivo*. Despite
293 evolving approaches for measurement of placental oxygenation, findings have varied widely
294 and adequate spatiotemporal resolution has so far been challenging[63]. However, it is apparent
295 that due to arteriovenous shunting and high metabolic extraction rates, the placenta
296 experiences hypoxia throughout pregnancy with a reported partial pressure of oxygen 30-50
297 mm Hg in the intervillous space, so perhaps a relevant question is what *prevents* HIF-1
298 stabilization and its downstream effects early in gestation. It is possible that the gestational-
299 age-dependent HIF-1 induction we observed reflects not a change in oxygen availability, but
300 rather a change in other HIF-regulatory factors such as nicotinamide adenine dinucleotide
301 (NAD^+) depletion, as has been demonstrated to occur in muscle and is accompanied by
302 metabolic reprogramming and mitochondrial decline[64]. Importantly, replenishment of NAD^+

303 was shown to restore markers of mitochondrial function in these aged cells, suggesting that
304 mitochondrial effects of HIF-1-driven aging are reversible in some systems. Separately, a recent
305 study which compared the miR-nomes of 1st- versus 3rd-trimester human placenta highlighted
306 differential expression of miRNAs with functional links to silencing of hypoxia response and
307 cellular senescence pathways in the first trimester[65]. Future investigations into the impact of
308 placental HIF-1 regulation will require a more precise understanding of placental oxygenation *in*
309 *vivo* and a sophisticated approach to model these factors in placental explants or other cellular
310 systems.
311
312 The shift in metabolic phenotype away from oxidative respiration in late pregnancy as
313 demonstrated by our transcriptomics analysis is consistent with earlier findings from
314 respirometry studies in mouse placenta[66], where rates of oxidative phosphorylation were noted
315 to decline from e14 to e19, particularly in the labyrinthine zone. It is still unclear if this shift
316 reflects changing substrate availability, or oxygen content, or perhaps the metabolic needs of
317 the developing fetus. A better understanding of the dynamic metabolism of the placenta across
318 gestation will be crucial for developing strategies for optimizing placental health, with major
319 implications for both maternal and fetal outcomes. For example, placental metabolomics
320 studies with a gestational time series could help corroborate the metabolic implications
321 interpreted from our transcriptomic data. And while our study stemmed from analysis of the
322 whole-organ placental transcriptome, single-cell transcriptomics across advancing gestational
323 age in healthy placentas would offer critical cell-type localization of specific metabolic events
324 noted to occur late in pregnancy.

325

326 Our data have implications for other adverse pregnancy outcomes beyond preterm birth,
327 including intrauterine growth restriction and preeclampsia. Two important recent studies have
328 examined separate mouse models with constitutively active placental HIF-1 and found that
329 when induced from the beginning of gestation, placental HIF-1 signaling drives abnormal
330 placentogenesis and impaired spiral artery remodeling, leading to placental hypoperfusion,
331 fetal growth restriction, and a preeclampsia-like clinical syndrome[67,68]. In the context of these
332 earlier results, our study highlights the critical gestational age-dependence of HIF-1 effects,
333 having demonstrated that in a normally developed mouse placenta, induction of HIF-1 signaling
334 during the final days of gestation leads to labor onset. Timing may be key to understanding how
335 two distinct pregnancy complications – preterm labor and preeclampsia – appear to emerge
336 separately from overlapping pathophysiologic mechanisms[69-73].

337

338 In summary, we report a molecular characterization of placental aging phenomena occurring in
339 normal pregnancies, stemming from induction of HIF-1 signaling and downstream
340 mitochondrial dysfunction and cellular senescence. These findings establish aging in the
341 placenta as a feature of normal gestation; identify HIF-1 signaling as an upstream trigger
342 leading to mitochondrial dysfunction and senescence in the placenta; demonstrate that the
343 secretome of senescent trophoblasts is sufficient to potentiate uterine myocyte transformation
344 and contractility; and establish that HIF-1 induction *in vivo* can induce preterm labor. These
345 findings may have important implications for illuminating the factors that determine gestational
346 length both in health and disease.

347

348 **Data Availability:**

349 Statistics accompanying WGCNA (Figure 2) are accessible through Mendeley Data, doi:

350 10.17632/g6vrw9jjn4.1. (https://data.mendeley.com/datasets/g6vrw9jjn4/1)

351

352 The RNA Seq dataset has been deposited in NCBI's Gene Expression Omnibus[21] and is accessible

353 through GEO Series accession number GSE199278.

354 (https://www.ncbi.nlm.nih.gov/geo/query/acc.cgi?acc=GSE199278)

355 Additional source data (original images for all blots) available in attached files.

356

357 **Methods:**

358 *Mouse placenta collection:* Wild-type C57BL/6 mice (Jackson Laboratory #000664) were fed a

359 chow diet and housed at 20°C in a 12-hour light/12-hour dark cycle. Nulliparous females (< 6

360 months of age) were housed for a single dark cycle (midnight = gestational day 0) with a stud

361 male. On gestational day e13.5-17.5, placentas were isolated via laparotomy from pregnant

362 females anesthetized via surgical-plane isoflurane. Placentas were quartered, immersion-rinsed

363 in dH_2O and blotted dry, then snap frozen in liquid nitrogen and stored at -80°C prior to use.

364

365 *Mouse trophoblast isolation:* Protocol described in full in Pennington *et al*[74]. On gestational day

366 e15.5, placentas were collected via laparotomy from pregnant wild-type C57BL/6 female mice

367 anesthetized with surgical-plane isoflurane. After dissection, placentas were quartered,

368 immersion-rinsed in dH2O, then placed in ice-cold digestion buffer: DMEM plus HEPES 20 mM,

369 collagenase 1mg/mL, and DNase I 4000U/mL. Placentas were digested for 20-40 minutes at
370 37°C with trituration and examined under a microscope until optimal digestion achieved.
371 Digested cells were passed through a 70 micron strainer, washed in DMEM, then separated
372 using a Percoll gradient. Trophoblast fraction was washed once more then plated in complete
373 medium: DMEM with HEPES 20 mM, FBS 10%, and supplemented with sodium pyruvate, pen-
374 strep-glutamine, non-essential amino acids, and gentamicin. Cells were grown at 37°C in 95%
375 ambient air with 5% CO_2.
376
377 *Mouse DMOG injection and measurement of gestational length*: On gestational day e16.5, dams
378 received an intraperitoneal injection of DMOG (Selleck Chemicals) 7.5 mg in 0.3 mL sterile
379 saline (approximately 250 mg/kg) versus vehicle alone. Video recordings were used to measure
380 gestational length, defined as interval from midnight of timed mating period until birth of the
381 first pup.
382
383 *Human placental specimens.* Placenta samples were collected at the time of cesarean delivery,
384 within 20 minutes of delivery of the placenta. Placental tissue was sampled from approximately
385 1cm deep to the maternal surface after dissecting away membranes. Cotyledons from all 4
386 quadrants were collected and minced together prior to immersion rinse in dH_2O and storage of
387 separate aliquots by snap freezing versus immersion in RNA Later. All samples were stored at -
388 80°C prior to use.
389
390 *Cell culture.*

391 All cells were grown at 37°C in 95% ambient air with 5% CO_2. JAR choriocarcinoma cells (ATCC
392 HTB-144; authenticated by STR profiling and confirmed negative for mycoplasma
393 contamination) were grown in RPMI 1640 media (4.5 g/L glucose) supplemented with 10% FBS.
394 Adherent JAR cells were treated with HIF1-stabilizing agents dissolved in 1X PBS (pH 7.4): cobalt
395 chloride hexahydrate (100 µM $CoCl_2$, Millipore Sigma) and dimethyloxalylglycine, N-
396 (methoxyoxoacetyl)-glycine methyl ester (1 mM DMOG, Millipore Sigma). JAR cells were
397 treated with 100 µM $CoCl_2$ or 1 mM DMOG in culture media as indicated prior to endpoint
398 assays.
399
400 Preparation of conditioned media: On day 5 of JAR cell treatment with $CoCl_2$ (versus control
401 condition), media exchange was performed to apply serum-free media for both conditions. 24
402 hours later, conditioned media samples were collected and applied to 10 kDa molecular weight
403 cutoff filters (Amicon Ultra), with centrifugation for 20 minutes at 4000 x *g*, 4°C. Filters were
404 washed with one volume of hTERT-HM base medium (see below), with repeat centrifugation.
405 Concentrated proteins retained in suspension above the filter were collected and stored at -
406 80°C.
407
408 hTERT-HM cells (generously supplied by Dr. Jennifer Condon, Wayne State; STR reference
409 profile not available) were grown in DMEM/F12 medium (Gibco) with 10% FBS and Antibiotic-
410 Antimycotic (1X, Gibco). Cells were stimulated by addition of recombinant human IL-1β (R&D
411 Systems) and/or filter-concentrated JAR cell conditioned media as indicated, 6 hours prior to
412 collection of cellular RNA.

413

414 *RT – qPCR*. Total RNA was reverse transcribed to cDNA with the Superscript III reverse
415 transcriptase (Invitrogen) system with random hexamer primers (Invitrogen) according to
416 manufacturer's instructions. cDNA was amplified via real-time quantitative PCR with TaqMan
417 Fast Advanced Master Mix (Applied Biosystems) or SYBR Green PCR Master mix (Qiagen) in a
418 QuantStudio 6 Flex Real-Time PCR System (Applied Biosystems). In mouse samples, target gene
419 expression was normalized to endogenous levels of housekeeping gene, β-actin. In human
420 samples, target gene expression was normalized to endogenous levels of housekeeping gene,
421 YWHAZ (TaqMan) or β-actin (SYBR). Mouse and human primers are listed in Table 2.

422

423 *Collagen lattice contraction assay*: As previously described[41,44], hTERT-HM cells were suspended
424 in a collagen gel matrix (Cellmatrix collagen type I-A, Fisher Scientific, prepared with MEM,
425 NaOH and HEPES) then plated in 12-well dishes and grown in hTERT-HM medium. When cells
426 reached approximately 60% confluence, gel matrix was detached from plate and experimental
427 treatments were applied in fresh cell culture medium. After 1 hour incubation, a photograph
428 was taken of each well for manual measurement of percent well area occupied by collagen disc
429 (using imageJ), reflecting cellular contraction.

430

431 *mtDNA damage assay.* Mitochondrial DNA damage was assayed from total DNA via a semi-long
432 run real-time PCR approach, as described elsewhere[32]. Briefly, separate qPCR reactions were
433 assayed to compare a long versus short amplicon representing each genomic region. A lesion
434 rate per 10 kb of mtDNA was calculated as:

435 lesion rate $= \frac{10000\ (bp)}{size\ of\ long\ fragment\ (bp)} * (1 - FC_{long-short})$,

436 with $FC_{long-short} = 2^{-\Delta\Delta Ct}$ calculated in the usual method.

437

438 *Relative mtDNA copy number.* qPCR assays for nuclear and mitochondrial genes were

439 performed using total DNA as a template. Relative mitochondrial DNA was calculated as:

440 follows:

441 mt:nuc DNA copy number $= 2 * 2^{\Delta Ct}$, where $\Delta Ct = Ct_{nuclear\ gene} - Ct_{mitochondrial\ gene}$.

442

443 *Immunoblots.* Protein extraction was performed on cell pellets using RIPA lysis buffer, or on

444 snap-frozen tissue using RIPA lysis buffer and a bead homogenizer. Protein lysates were

445 fractionated using NuPage Bis-Tris polyacrylamide gels (20μg total protein per well) and

446 transferred to PVDF membranes. Antibodies are listed in Table 3.

447

448 *SA-β-Galactosidase Assay.* Adherent cells were fixed and stained for SA-βGal via a Senescence

449 Detection kit (Abcam, ab65351) per manufacturer's instructions. Representative images were

450 used to calculate the fraction of SA-β-Gal-positive cells, scored by an observer blinded to

451 treatment condition.

452

453 *Live cell staining.* Adherent cells were stained using the TMRE-Mitochondrial Membrane

454 Potential Assay Kit (Abcam, ab113852) per manufacturer's instructions. Select wells were

455 pretreated with 20 μM FCCP, a decoupling agent, as a positive control for 20 minutes before

456 TMRE and Hoechst counterstain was applied. Live JAR cells were analyzed by the Celigo Image

457 Cytometer (Nexcelom BioScience) for fluorescence quantification and gating. Adherent live JAR
458 cells were stained with MitoSOX™ Red Mitochondrial Superoxide Indicator kit (Invitrogen) and
459 analyzed using the cytometer in a similar manner.
460
461 *Cell counting.* JAR cells were cultured for 6 days ± cobalt chloride exposure prior to cell
462 counting. On day 6, cells from each condition were replated in a 96-well plate in $CoCl_2$-free
463 media at a density of 5 x 10^3 cells per well. Celigo Image Cytometer was used for automated cell
464 counting (total cells per well) at 24-hour intervals.
465
466 *RNA-Seq.* Following 6 days of treatment with CoCl2 100 μM versus control media, total RNA was
467 isolated from JAR cells as described above. Extracted RNA (300ng) was treated with NEBNext
468 rRNA Depletion Kit v2 (E7400X) and cDNA was generated using random hexamer priming and
469 Maxima H Minus Reverse Transcriptase. cDNA was converted into double stranded cDNA using
470 NEBNext mRNA Second Strand Synthesis Module (E6111L) and sequencing libraries were
471 generated by tagmentation using Nextera XT DNA Library Preparation Kit (Illumina FC-131) with
472 12 cycles of PCR amplification. Sequencing libraries were analyzed by Qubit and Agilent
473 Bioanalyzer, pooled at a final concentration of 1.2pM, and sequenced on an Illumina
474 Nextseq500 instrument 36x8x36 read structure.
475
476 *Transcriptomics Analysis*: Sequencing reads were demultiplexed and trimmed for adapters
477 using bcl2fastq (v2.20.0). Secondary adapter trimming, NextSeq/Poly(G) tail trimming, and read
478 filtering was performed using fastp (v0.20.0)[75]; low quality reads and reads shorter than 18nt

479 after trimming were removed from the read pool. Salmon (v1.1.0)[76] was used to simultaneously
480 map and quantify reads to transcripts in the GENCODE 33 genome annotation of the
481 GRCh38/hg38 human assembly. Salmon was run using full selective alignment, with sequence-
482 specific and fragment GC-bias correction turned on (--seqBias and --gcBias options,
483 respectively). Transcript abundances were collated and summarized to gene abundances using
484 the tximport package for R[77]. Normalization and differential expression analysis were
485 performed using edgeR[78,79]. For differential gene expression analysis, genes were considered
486 significant if they passed a fold change (FC) cutoff of log2FC > 1 and a false discovery rate (FDR)
487 cutoff of FDR < 0.05. Functional enrichment analyses were performed using g:Profiler[80].
488 WGCNA[81] was performed after removing genes with low expression as previously described[82].
489
490 *Statistics.* Student's two-tailed unpaired t-test, ordinary one-way, and two-way ANOVA
491 statistical tests were applied as indicated to compare biological replicates in each experiment.
492 Data were excluded as outliers using the interquartile range method (lower limit = 1st quartile –
493 1.5 x IQR; upper limit = 3rd quartile + 1.5 x IQR).
494
495 *Study Approval.* All animal experiments were approved by the Beth Israel Deaconess Medical
496 Center Institutional Animal Care and Use Committee (protocol #008-2022). Human placental
497 specimens and data were biobanked and accessed under protocols approved by the Beth Israel
498 Deaconess Medical Center Institutional Review Board, and written informed consent was
499 obtained before subject participation (protocols #2008P000061, 2020P000997, 2021P000897).
500

Acknowledgements:

We thank Dr. Jennifer Condon of Wayne State University School of Medicine for generously providing the hTERT-HM cell line.

We thank Saira Salahuddin for maintaining the placenta biorepository and helping access the study samples and accompanying clinical data.

Figures were created using Biorender.com.

Research reported in this publication was supported by the Institute of General Medical Sciences of the National Institutes of Health under award GM007592-41 and the Foundation for Anesthesia Education and Research (FAER) (EJC).

The authors declare no competing interests.

518 **References:**

519 1. Liu, L., Oza, S., Hogan, D., Perin, J., Rudan, I., Lawn, J.E., Cousens, S., Mathers, C., and
520 Black, R.E. (2015). Global, regional, and national causes of child mortality in 2000-13,
521 with projections to inform post-2015 priorities: an updated systematic analysis. Lancet
522 *385*, 430-440. 10.1016/S0140-6736(14)61698-6.
523 2. Blencowe, H., Cousens, S., Chou, D., Oestergaard, M., Say, L., Moller, A.B., Kinney, M.,
524 Lawn, J., and Born Too Soon Preterm Birth Action, G. (2013). Born too soon: the global
525 epidemiology of 15 million preterm births. Reprod Health *10 Suppl 1*, S2. 10.1186/1742-
526 4755-10-S1-S2.
527 3. Goldenberg, R.L., Culhane, J.F., Iams, J.D., and Romero, R. (2008). Epidemiology and
528 causes of preterm birth. Lancet *371*, 75-84. 10.1016/S0140-6736(08)60074-4.
529 4. Smith, V., Devane, D., Begley, C.M., Clarke, M., and Higgins, S. (2009). A systematic
530 review and quality assessment of systematic reviews of randomised trials of
531 interventions for preventing and treating preterm birth. Eur J Obstet Gynecol Reprod
532 Biol *142*, 3-11. 10.1016/j.ejogrb.2008.09.008.
533 5. Romero, R., Dey, S.K., and Fisher, S.J. (2014). Preterm labor: one syndrome, many
534 causes. Science *345*, 760-765. 10.1126/science.1251816.
535 6. Kiserud, T., Ebbing, C., Kessler, J., and Rasmussen, S. (2006). Fetal cardiac output,
536 distribution to the placenta and impact of placental compromise. Ultrasound Obstet
537 Gynecol *28*, 126-136. 10.1002/uog.2832.
538 7. Shaut, C.A., Keene, D.R., Sorensen, L.K., Li, D.Y., and Stadler, H.S. (2008). HOXA13 Is
539 essential for placental vascular patterning and labyrinth endothelial specification. PLoS
540 Genet *4*, e1000073. 10.1371/journal.pgen.1000073.
541 8. Lykke, J.A., Langhoff-Roos, J., Sibai, B.M., Funai, E.F., Triche, E.W., and Paidas, M.J.
542 (2009). Hypertensive pregnancy disorders and subsequent cardiovascular morbidity and
543 type 2 diabetes mellitus in the mother. Hypertension *53*, 944-951.
544 10.1161/HYPERTENSIONAHA.109.130765.
545 9. Genbacev, O., Joslin, R., Damsky, C.H., Polliotti, B.M., and Fisher, S.J. (1996). Hypoxia
546 alters early gestation human cytotrophoblast differentiation/invasion in vitro and
547 models the placental defects that occur in preeclampsia. J Clin Invest *97*, 540-550.
548 10.1172/JCI118447.
549 10. Plaks, V., Rinkenberger, J., Dai, J., Flannery, M., Sund, M., Kanasaki, K., Ni, W., Kalluri, R.,
550 and Werb, Z. (2013). Matrix metalloproteinase-9 deficiency phenocopies features of
551 preeclampsia and intrauterine growth restriction. Proc Natl Acad Sci U S A *110*, 11109-
552 11114. 10.1073/pnas.1309561110.
553 11. Li, F., Fushima, T., Oyanagi, G., Townley-Tilson, H.W., Sato, E., Nakada, H., Oe, Y.,
554 Hagaman, J.R., Wilder, J., Li, M., et al. (2016). Nicotinamide benefits both mothers and
555 pups in two contrasting mouse models of preeclampsia. Proc Natl Acad Sci U S A *113*,
556 13450-13455. 10.1073/pnas.1614947113.
557 12. Romero, R., and Chaiworapongsa, T. (2013). Preeclampsia: a link between trophoblast
558 dysregulation and an antiangiogenic state. J Clin Invest *123*, 2775-2777.
559 10.1172/JCI70431.

560 13. McIntyre, K.R., Vincent, K.M.M., Hayward, C.E., Li, X., Sibley, C.P., Desforges, M.,
561 Greenwood, S.L., and Dilworth, M.R. (2020). Human placental uptake of glutamine and
562 glutamate is reduced in fetal growth restriction. Sci Rep *10*, 16197. 10.1038/s41598-
563 020-72930-7.
564 14. Xu, Y.Y., Liu, Y., Cui, L., Wu, W.B., Quinn, M.J., Menon, R., and Zhang, H.J. (2021).
565 Hypoxic effects on the mitochondrial content and functions of the placenta in fetal
566 growth restriction. Placenta *114*, 100-107. 10.1016/j.placenta.2021.09.003.
567 15. Koga, K., Cardenas, I., Aldo, P., Abrahams, V.M., Peng, B., Fill, S., Romero, R., and Mor, G.
568 (2009). Activation of TLR3 in the trophoblast is associated with preterm delivery. Am J
569 Reprod Immunol *61*, 196-212. 10.1111/j.1600-0897.2008.00682.x.
570 16. Pique-Regi, R., Romero, R., Tarca, A.L., Sendler, E.D., Xu, Y., Garcia-Flores, V., Leng, Y.,
571 Luca, F., Hassan, S.S., and Gomez-Lopez, N. (2019). Single cell transcriptional signatures
572 of the human placenta in term and preterm parturition. Elife *8*. 10.7554/eLife.52004.
573 17. Beharier, O., Tyurin, V.A., Goff, J.P., Guerrero-Santoro, J., Kajiwara, K., Chu, T., Tyurina,
574 Y.Y., St Croix, C.M., Wallace, C.T., Parry, S., et al. (2020). PLA2G6 guards placental
575 trophoblasts against ferroptotic injury. Proc Natl Acad Sci U S A *117*, 27319-27328.
576 10.1073/pnas.2009201117.
577 18. Elshenawy, S., Pinney, S.E., Stuart, T., Doulias, P.T., Zura, G., Parry, S., Elovitz, M.A.,
578 Bennett, M.J., Bansal, A., Strauss, J.F., 3rd, et al. (2020). The Metabolomic Signature of
579 the Placenta in Spontaneous Preterm Birth. Int J Mol Sci *21*. 10.3390/ijms21031043.
580 19. Lien, Y.C., Zhang, Z., Cheng, Y., Polyak, E., Sillers, L., Falk, M.J., Ischiropoulos, H., Parry, S.,
581 and Simmons, R.A. (2021). Human Placental Transcriptome Reveals Critical Alterations in
582 Inflammation and Energy Metabolism with Fetal Sex Differences in Spontaneous
583 Preterm Birth. Int J Mol Sci *22*. 10.3390/ijms22157899.
584 20. Paquette, A.G., Brockway, H.M., Price, N.D., and Muglia, L.J. (2018). Comparative
585 transcriptomic analysis of human placentae at term and preterm delivery. Biol Reprod
586 *98*, 89-101. 10.1093/biolre/iox163.
587 21. Edgar, R., Domrachev, M., and Lash, A.E. (2002). Gene Expression Omnibus: NCBI gene
588 expression and hybridization array data repository. Nucleic Acids Res *30*, 207-210.
589 10.1093/nar/30.1.207.
590 22. Knox, K., and Baker, J.C. (2008). Genomic evolution of the placenta using co-option and
591 duplication and divergence. Genome Res *18*, 695-705. 10.1101/gr.071407.107.
592 23. Zhou, Q.Y., Fang, M.D., Huang, T.H., Li, C.C., Yu, M., and Zhao, S.H. (2009). Detection of
593 differentially expressed genes between Erhualian and Large White placentas on day 75
594 and 90 of gestation. BMC Genomics *10*, 337. 10.1186/1471-2164-10-337.
595 24. Loux, S.C., Dini, P., El-Sheikh Ali, H., Kalbfleisch, T., and Ball, B.A. (2019). Characterization
596 of the placental transcriptome through mid to late gestation in the mare. PLoS One *14*,
597 e0224497. 10.1371/journal.pone.0224497.
598 25. Soncin, F., Khater, M., To, C., Pizzo, D., Farah, O., Wakeland, A., Arul Nambi Rajan, K.,
599 Nelson, K.K., Chang, C.W., Moretto-Zita, M., et al. (2018). Comparative analysis of
600 mouse and human placentae across gestation reveals species-specific regulators of
601 placental development. Development *145*. 10.1242/dev.156273.
602 26. Maeda, K.J., Showmaker, K.C., Johnson, A.C., Garrett, M.R., and Sasser, J.M. (2019).
603 Spontaneous superimposed preeclampsia: chronology and expression unveiled by

604 temporal transcriptomic analysis. Physiol Genomics *51*, 342-355.
605 10.1152/physiolgenomics.00020.2019.
606 27. Morey, R., Farah, O., Kallol, S., Requena, D.F., Meads, M., Moretto-Zita, M., Soncin, F.,
607 Laurent, L.C., and Parast, M.M. (2021). Transcriptomic Drivers of Differentiation,
608 Maturation, and Polyploidy in Human Extravillous Trophoblast. Front Cell Dev Biol *9*,
609 702046. 10.3389/fcell.2021.702046.
610 28. Steinhauser, C.B., Lambo, C.A., Askelson, K., Burns, G.W., Behura, S.K., Spencer, T.E.,
611 Bazer, F.W., and Satterfield, M.C. (2021). Placental Transcriptome Adaptations to
612 Maternal Nutrient Restriction in Sheep. Int J Mol Sci *22*. 10.3390/ijms22147654.
613 29. Lee, B.Y., Han, J.A., Im, J.S., Morrone, A., Johung, K., Goodwin, E.C., Kleijer, W.J., DiMaio,
614 D., and Hwang, E.S. (2006). Senescence-associated beta-galactosidase is lysosomal beta-
615 galactosidase. Aging Cell *5*, 187-195. 10.1111/j.1474-9726.2006.00199.x.
616 30. Jang, J.Y., Blum, A., Liu, J., and Finkel, T. (2018). The role of mitochondria in aging. J Clin
617 Invest *128*, 3662-3670. 10.1172/JCI120842.
618 31. Trifunovic, A., Wredenberg, A., Falkenberg, M., Spelbrink, J.N., Rovio, A.T., Bruder, C.E.,
619 Bohlooly, Y.M., Gidlof, S., Oldfors, A., Wibom, R., et al. (2004). Premature ageing in mice
620 expressing defective mitochondrial DNA polymerase. Nature *429*, 417-423.
621 10.1038/nature02517.
622 32. Rothfuss, O., Gasser, T., and Patenge, N. (2010). Analysis of differential DNA damage in
623 the mitochondrial genome employing a semi-long run real-time PCR approach. Nucleic
624 Acids Res *38*, e24. 10.1093/nar/gkp1082.
625 33. Bratic, A., and Larsson, N.G. (2013). The role of mitochondria in aging. J Clin Invest *123*,
626 951-957. 10.1172/JCI64125.
627 34. Wiley, C.D., and Campisi, J. (2016). From Ancient Pathways to Aging Cells-Connecting
628 Metabolism and Cellular Senescence. Cell Metab *23*, 1013-1021.
629 10.1016/j.cmet.2016.05.010.
630 35. Wiley, C.D., and Campisi, J. (2021). The metabolic roots of senescence: mechanisms and
631 opportunities for intervention. Nat Metab *3*, 1290-1301. 10.1038/s42255-021-00483-8.
632 36. Maxwell, P.H., Wiesener, M.S., Chang, G.W., Clifford, S.C., Vaux, E.C., Cockman, M.E.,
633 Wykoff, C.C., Pugh, C.W., Maher, E.R., and Ratcliffe, P.J. (1999). The tumour suppressor
634 protein VHL targets hypoxia-inducible factors for oxygen-dependent proteolysis. Nature
635 *399*, 271-275. 10.1038/20459.
636 37. Jaakkola, P., Mole, D.R., Tian, Y.M., Wilson, M.I., Gielbert, J., Gaskell, S.J., von
637 Kriegsheim, A., Hebestreit, H.F., Mukherji, M., Schofield, C.J., et al. (2001). Targeting of
638 HIF-alpha to the von Hippel-Lindau ubiquitylation complex by O2-regulated prolyl
639 hydroxylation. Science *292*, 468-472. 10.1126/science.1059796.
640 38. Nursalim, Y.N.S., Blenkiron, C., Groom, K.M., and Chamley, L.W. (2020). Growing human
641 trophoblasts in vitro: a review of the media commonly used in trophoblast cell culture.
642 Reproduction *160*, R119-R128. 10.1530/REP-19-0605.
643 39. Rothbauer, M., Patel, N., Gondola, H., Siwetz, M., Huppertz, B., and Ertl, P. (2017). A
644 comparative study of five physiological key parameters between four different human
645 trophoblast-derived cell lines. Sci Rep *7*, 5892. 10.1038/s41598-017-06364-z.
646 40. Epstein, A.C., Gleadle, J.M., McNeill, L.A., Hewitson, K.S., O'Rourke, J., Mole, D.R.,
647 Mukherji, M., Metzen, E., Wilson, M.I., Dhanda, A., et al. (2001). C. elegans EGL-9 and

648 mammalian homologs define a family of dioxygenases that regulate HIF by prolyl
649 hydroxylation. Cell *107*, 43-54. 10.1016/s0092-8674(01)00507-4.
650 41. Nishimura, F., Mogami, H., Moriuchi, K., Chigusa, Y., Mandai, M., and Kondoh, E. (2020).
651 Mechanisms of thrombin-Induced myometrial contractions: Potential targets of
652 progesterone. PLoS One *15*, e0231944. 10.1371/journal.pone.0231944.
653 42. Rauk, P.N., and Chiao, J.P. (2000). Interleukin-1 stimulates human uterine prostaglandin
654 production through induction of cyclooxygenase-2 expression. Am J Reprod Immunol
655 *43*, 152-159. 10.1111/j.8755-8920.2000.430304.x.
656 43. Leimert, K.B., Verstraeten, B.S.E., Messer, A., Nemati, R., Blackadar, K., Fang, X.,
657 Robertson, S.A., Chemtob, S., and Olson, D.M. (2019). Cooperative effects of sequential
658 PGF2alpha and IL-1beta on IL-6 and COX-2 expression in human myometrial cellsdagger.
659 Biol Reprod *100*, 1370-1385. 10.1093/biolre/ioz029.
660 44. Devost, D., and Zingg, H.H. (2007). Novel in vitro system for functional assessment of
661 oxytocin action. Am J Physiol Endocrinol Metab *292*, E1-6.
662 10.1152/ajpendo.00529.2005.
663 45. Campisi, J., Kapahi, P., Lithgow, G.J., Melov, S., Newman, J.C., and Verdin, E. (2019).
664 From discoveries in ageing research to therapeutics for healthy ageing. Nature *571*, 183-
665 192. 10.1038/s41586-019-1365-2.
666 46. Rosso, P. (1976). Placenta as an aging organ. Curr Concepts Nutr *4*, 23-41.
667 47. Martin, B.J., and Spicer, S.S. (1973). Ultrastructural features of cellular maturation and
668 aging in human trophoblast. J Ultrastruct Res *43*, 133-149. 10.1016/s0022-
669 5320(73)90074-9.
670 48. Fox, H. (1997). Aging of the placenta. Arch Dis Child Fetal Neonatal Ed *77*, F171-175.
671 10.1136/fn.77.3.f171.
672 49. Sultana, Z., Maiti, K., Aitken, J., Morris, J., Dedman, L., and Smith, R. (2017). Oxidative
673 stress, placental ageing-related pathologies and adverse pregnancy outcomes. Am J
674 Reprod Immunol *77*. 10.1111/aji.12653.
675 50. Cindrova-Davies, T., Fogarty, N.M.E., Jones, C.J.P., Kingdom, J., and Burton, G.J. (2018).
676 Evidence of oxidative stress-induced senescence in mature, post-mature and
677 pathological human placentas. Placenta *68*, 15-22. 10.1016/j.placenta.2018.06.307.
678 51. Biron-Shental, T., Sukenik-Halevy, R., Sharon, Y., Goldberg-Bittman, L., Kidron, D., Fejgin,
679 M.D., and Amiel, A. (2010). Short telomeres may play a role in placental dysfunction in
680 preeclampsia and intrauterine growth restriction. Am J Obstet Gynecol *202*, 381 e381-
681 387. 10.1016/j.ajog.2010.01.036.
682 52. Chen, K.H., Chen, L.R., and Lee, Y.H. (2011). Exploring the relationship between preterm
683 placental calcification and adverse maternal and fetal outcome. Ultrasound Obstet
684 Gynecol *37*, 328-334. 10.1002/uog.7733.
685 53. Maiti, K., Sultana, Z., Aitken, R.J., Morris, J., Park, F., Andrew, B., Riley, S.C., and Smith, R.
686 (2017). Evidence that fetal death is associated with placental aging. Am J Obstet Gynecol
687 *217*, 441 e441-441 e414. 10.1016/j.ajog.2017.06.015.
688 54. Bonney, E.A., Krebs, K., Saade, G., Kechichian, T., Trivedi, J., Huaizhi, Y., and Menon, R.
689 (2016). Differential senescence in feto-maternal tissues during mouse pregnancy.
690 Placenta *43*, 26-34. 10.1016/j.placenta.2016.04.018.

691 55. Menon, R., Behnia, F., Polettini, J., Saade, G.R., Campisi, J., and Velarde, M. (2016).
692 Placental membrane aging and HMGB1 signaling associated with human parturition.
693 Aging (Albany NY) *8*, 216-230. 10.18632/aging.100891.
694 56. Menon, R., Richardson, L.S., and Lappas, M. (2019). Fetal membrane architecture, aging
695 and inflammation in pregnancy and parturition. Placenta *79*, 40-45.
696 10.1016/j.placenta.2018.11.003.
697 57. Sheller-Miller, S., Trivedi, J., Yellon, S.M., and Menon, R. (2019). Exosomes Cause
698 Preterm Birth in Mice: Evidence for Paracrine Signaling in Pregnancy. Sci Rep *9*, 608.
699 10.1038/s41598-018-37002-x.
700 58. Migale, R., Herbert, B.R., Lee, Y.S., Sykes, L., Waddington, S.N., Peebles, D., Hagberg, H.,
701 Johnson, M.R., Bennett, P.R., and MacIntyre, D.A. (2015). Specific Lipopolysaccharide
702 Serotypes Induce Differential Maternal and Neonatal Inflammatory Responses in a
703 Murine Model of Preterm Labor. Am J Pathol *185*, 2390-2401.
704 10.1016/j.ajpath.2015.05.015.
705 59. Srikhajon, K., Shynlova, O., Preechapornprasert, A., Chanrachakul, B., and Lye, S. (2014).
706 A new role for monocytes in modulating myometrial inflammation during human labor.
707 Biol Reprod *91*, 10. 10.1095/biolreprod.113.114975.
708 60. Gomez-Lopez, N., StLouis, D., Lehr, M.A., Sanchez-Rodriguez, E.N., and Arenas-
709 Hernandez, M. (2014). Immune cells in term and preterm labor. Cell Mol Immunol *11*,
710 571-581. 10.1038/cmi.2014.46.
711 61. Hirota, Y., Daikoku, T., Tranguch, S., Xie, H., Bradshaw, H.B., and Dey, S.K. (2010).
712 Uterine-specific p53 deficiency confers premature uterine senescence and promotes
713 preterm birth in mice. J Clin Invest *120*, 803-815. 10.1172/JCI40051.
714 62. Hirota, Y., Cha, J., Yoshie, M., Daikoku, T., and Dey, S.K. (2011). Heightened uterine
715 mammalian target of rapamycin complex 1 (mTORC1) signaling provokes preterm birth
716 in mice. Proc Natl Acad Sci U S A *108*, 18073-18078. 10.1073/pnas.1108180108.
717 63. Nye, G.A., Ingram, E., Johnstone, E.D., Jensen, O.E., Schneider, H., Lewis, R.M.,
718 Chernyavsky, I.L., and Brownbill, P. (2018). Human placental oxygenation in late
719 gestation: experimental and theoretical approaches. J Physiol *596*, 5523-5534.
720 10.1113/JP275633.
721 64. Gomes, A.P., Price, N.L., Ling, A.J., Moslehi, J.J., Montgomery, M.K., Rajman, L., White,
722 J.P., Teodoro, J.S., Wrann, C.D., Hubbard, B.P., et al. (2013). Declining NAD(+) induces a
723 pseudohypoxic state disrupting nuclear-mitochondrial communication during aging. Cell
724 *155*, 1624-1638. 10.1016/j.cell.2013.11.037.
725 65. Gonzalez, T.L., Eisman, L.E., Joshi, N.V., Flowers, A.E., Wu, D., Wang, Y., Santiskulvong,
726 C., Tang, J., Buttle, R.A., Sauro, E., et al. (2021). High-throughput miRNA sequencing of
727 the human placenta: expression throughout gestation. Epigenomics *13*, 995-1012.
728 10.2217/epi-2021-0055.
729 66. Sferruzzi-Perri, A.N., Higgins, J.S., Vaughan, O.R., Murray, A.J., and Fowden, A.L. (2019).
730 Placental mitochondria adapt developmentally and in response to hypoxia to support
731 fetal growth. Proc Natl Acad Sci U S A *116*, 1621-1626. 10.1073/pnas.1816056116.
732 67. Albers, R.E., Kaufman, M.R., Natale, B.V., Keoni, C., Kulkarni-Datar, K., Min, S., Williams,
733 C.R., Natale, D.R.C., and Brown, T.L. (2019). Trophoblast-Specific Expression of Hif-

734 1alpha Results in Preeclampsia-Like Symptoms and Fetal Growth Restriction. Sci Rep *9*,
735 2742. 10.1038/s41598-019-39426-5.
736 68. Sallais, J., Park, C., Alahari, S., Porter, T., Liu, R., Kurt, M., Farrell, A., Post, M., and
737 Caniggia, I. (2022). HIF1 inhibitor acriflavine rescues early-onset preeclampsia
738 phenotype in mice lacking placental prolyl hydroxylase domain protein 2. JCI Insight *7*.
739 10.1172/jci.insight.158908.
740 69. Rasmussen, S., Ebbing, C., and Irgens, L.M. (2017). Predicting preeclampsia from a
741 history of preterm birth. PLoS One *12*, e0181016. 10.1371/journal.pone.0181016.
742 70. Mando, C., De Palma, C., Stampalija, T., Anelli, G.M., Figus, M., Novielli, C., Parisi, F.,
743 Clementi, E., Ferrazzi, E., and Cetin, I. (2014). Placental mitochondrial content and
744 function in intrauterine growth restriction and preeclampsia. Am J Physiol Endocrinol
745 Metab *306*, E404-413. 10.1152/ajpendo.00426.2013.
746 71. Fujimaki, A., Watanabe, K., Mori, T., Kimura, C., Shinohara, K., and Wakatsuki, A. (2011).
747 Placental oxidative DNA damage and its repair in preeclamptic women with fetal growth
748 restriction. Placenta *32*, 367-372. 10.1016/j.placenta.2011.02.004.
749 72. Davy, P., Nagata, M., Bullard, P., Fogelson, N.S., and Allsopp, R. (2009). Fetal growth
750 restriction is associated with accelerated telomere shortening and increased expression
751 of cell senescence markers in the placenta. Placenta *30*, 539-542.
752 10.1016/j.placenta.2009.03.005.
753 73. Burton, G.J., Yung, H.W., Cindrova-Davies, T., and Charnock-Jones, D.S. (2009). Placental
754 endoplasmic reticulum stress and oxidative stress in the pathophysiology of unexplained
755 intrauterine growth restriction and early onset preeclampsia. Placenta *30 Suppl A*, S43-
756 48. 10.1016/j.placenta.2008.11.003.
757 74. Pennington, K.A., Schlitt, J.M., and Schulz, L.C. (2012). Isolation of primary mouse
758 trophoblast cells and trophoblast invasion assay. J Vis Exp, e3202. 10.3791/3202.
759 75. Chen, S., Zhou, Y., Chen, Y., and Gu, J. (2018). fastp: an ultra-fast all-in-one FASTQ
760 preprocessor. Bioinformatics *34*, i884-i890. 10.1093/bioinformatics/bty560.
761 76. Patro, R., Duggal, G., Love, M.I., Irizarry, R.A., and Kingsford, C. (2017). Salmon provides
762 fast and bias-aware quantification of transcript expression. Nat Methods *14*, 417-419.
763 10.1038/nmeth.4197.
764 77. Soneson, C., Love, M.I., and Robinson, M.D. (2015). Differential analyses for RNA-seq:
765 transcript-level estimates improve gene-level inferences. F1000Res *4*, 1521.
766 10.12688/f1000research.7563.2.
767 78. Robinson, M.D., McCarthy, D.J., and Smyth, G.K. (2010). edgeR: a Bioconductor package
768 for differential expression analysis of digital gene expression data. Bioinformatics *26*,
769 139-140. 10.1093/bioinformatics/btp616.
770 79. Chen, Y., Lun, A.T., and Smyth, G.K. (2016). From reads to genes to pathways:
771 differential expression analysis of RNA-Seq experiments using Rsubread and the edgeR
772 quasi-likelihood pipeline. F1000Res *5*, 1438. 10.12688/f1000research.8987.2.
773 80. Raudvere, U., Kolberg, L., Kuzmin, I., Arak, T., Adler, P., Peterson, H., and Vilo, J. (2019).
774 g:Profiler: a web server for functional enrichment analysis and conversions of gene lists
775 (2019 update). Nucleic Acids Res *47*, W191-W198. 10.1093/nar/gkz369.
776 81. Langfelder, P., and Horvath, S. (2008). WGCNA: an R package for weighted correlation
777 network analysis. BMC Bioinformatics *9*, 559. 10.1186/1471-2105-9-559.

82. Bentsen, M.A., Rausch, D.M., Mirzadeh, Z., Muta, K., Scarlett, J.M., Brown, J.M., Herranz-Perez, V., Baquero, A.F., Thompson, J., Alonge, K.M., et al. (2020). Transcriptomic analysis links diverse hypothalamic cell types to fibroblast growth factor 1-induced sustained diabetes remission. Nat Commun *11*, 4458. 10.1038/s41467-020-17720-5.

785 Figure Legends

786 **Figure 1. Systematic search flow for placental transcriptomics datasets.** 326 GEO datasets
787 were identified by the search terms "placenta" and "transcriptome"; nine met criteria for
788 containing placental transcriptomic data representing normal physiology at a range of
789 gestational timepoints spanning through the final 1/3 of pregnancy. Dataset selected for further
790 analysis in yellow.

791

792 **Figure 2. Mouse placental aging is characterized by cellular senescence, HIF-1 signaling, and**
793 **mitochondrial dysregulation.** WGCNA yielded 20 gene clusters. Functional pathways
794 overrepresented in clusters found to increase (blue) and decrease (turquoise) across gestation
795 highlight enhanced cellular senescence, increased HIF-1 signaling, and decreased mitochondrial
796 synthesis and respiration late in pregnancy (A). mRNA expression of senescence marker *Glb1*
797 peaks at e17.5 (B; one-way ANOVA p=0.0048). HIF-1 protein abundance is higher at e17.5
798 versus e13.5 and e15.5 (C; one-way ANOVA p=0.019), as is expression of HIF-1 targets *Hk2* and
799 *Slc2a1* (D; two-way ANOVA p<0.0001 for gestational age factor). (See Figure 2 - Supplement 1
800 for analysis of gene expression changes across timepoints by placental sex.) Mitochondrial
801 abundance, reflected by COX IV protein, decreases with gestational age (E, one-way ANOVA
802 p=0.0064), and mitochondrial DNA lesion rate peaks at e17.5 in the regions of the D-loop (one-
803 way ANOVA p=0.0001), COII/ATPase6 (p=0.0027), and ND5 (p=0.036) (F). B-F, Each data point
804 represents a biological replicate (eg. RNA, protein, or DNA extracted from an individual
805 placenta, in turn collected from one of 2-4 pregnant dams per group). Data normalized to mean
806 at e13.5. See Figure 2 - Source Data 1 for uncropped blots.

807

808 **Figure 2 - Supplement 1. Gestational age-dependent variability in expression of Hif-1 target**

809 ***Slc2a1*, but not *Hk2*, is affected by placental sex.** Subgroup analysis did not reveal sex-

810 dependent mRNA expression changes in *Glb1* (A) or *Hk2* (B) by qPCR, but did demonstrate

811 consistently higher *Slc2a1* expression in male placentas at all gestational ages and an

812 interaction between the effects of sex and gestational age on *Slc2a1* expression (C; two-way

813 ANOVA $p<0.0001$ for sex, $p<0.0001$ for gestational age, and $p=0.028$ for interaction). Each data

814 point represents a biological replicate (RNA isolated from an individual placenta, collected from

815 one of 2-4 dams per group). Data normalized to collective (M+F) mean at e13.5.

816

817 **Figure 2 - Source Data 1.** Uncropped, unedited blots from 2c (left) and 2e (right).

818

819 **Figure 3. Senescence, HIF-1 signaling, and decreased mitochondrial abundance characterize**

820 **late-gestation human placenta.** mRNA expression of senescence marker *GLB1* and HIF-1

821 targets *HK2* and *SLC2A1* trends higher in placentas from > 39-week cohort vs < 35-week cohort

822 (A; 2-way ANOVA gestational age factor $p=0.057$). Mitochondrial abundance, reflected by

823 mitochondrial genes *ATP6* and *COX2* (B; two-way ANOVA gestational age factor $p=0.042$) and

824 COX IV protein (C; $p=0.0036$) decreases with advancing gestational age. Each data point

825 represents a biological replicate (RNA or protein isolated from an individual placenta). Data

826 normalized to mean in < 35 week group. See Figure 3 - Source Data 1 for uncropped blots.

827

828 **Figure 3 - Source Data 1**. Uncropped, unedited blots from Figure 3.

829

830

831 **Figure 4. Short-term HIF-1 stabilization in primary mouse trophoblasts leads to decreased**

832 **mitochondrial abundance and cellular senescence.** HIF-1 is detected in cultured trophoblasts

833 exposed to $CoCl_2$ (A). After 48 hours of $CoCl_2$ exposure, trophoblasts exhibit decreased

834 mitochondrial abundance reflected by *Cox2* mRNA expression levels (B; p=0.014) and COX IV

835 protein levels (C; p=0.0047). Senescence marker *Glb1* is increased (D; p=0.038) and SA-βGal

836 accumulation is noted by X-gal assay (E; p=0.012). Each data point represents a technical

837 replicate (eg. protein, RNA, or β-Gal measured from an individual well of cells grown in treated

838 or control condition). Data normalized to mean of control treatment group. See Figure 4 -

839 Source Data 1 for uncropped blots.

840

841 **Figure 4 - Source Data 1**. Uncropped, unedited blots from 4a (left) and 4c (right)

842

843 **Figure 5. Long-term HIF-1 stabilization in JAR cells leads to mitochondrial dysfunction, cellular**

844 **senescence, and metabolic reprogramming.** HIF-1 is stabilized at 6 day timepoint of $CoCl_2$

845 exposure (A). After 6 days, mitochondrial abundance is decreased as reflected by a drop in the

846 mitochondrial:nuclear DNA copy number (B) and a decrease in COX IV protein (C). (See Figure 5

847 - Supplement 1 for timecourse of declining mitochondrial abundance.) Cells also exhibit

848 augmented signs of mitochondrial dysfunction via MtSox (D; p=0.0003) and TMRE staining (E;

849 two-way ANOVA CoCl2 factor p<0.0001). SA-βGal staining reflects a high proportion of

850 senescent cells (F; p<0.0001) and growth arrest is confirmed by cell counting following a 6-day

851 pre-treatment with $CoCl_2$ (G; two-way ANOVA $p<0.0001$ for interaction of $CoCl_2$ factor with
852 time). (See Figure 5 - Supplement 2 for assessment of cell death by propidium iodide staining.)
853 mRNA expression of SASP candidates *VEGF, TNFA, IL1A*, and *IL10* is altered after $CoCl_2$ exposure
854 (H; *, adjusted $p<0.01$). RNA Seq revealed upregulation of 2188 and downregulation of 1389
855 genes (I; genes with | log2(FC) | > 1 and -log(FDR)>2 indicated in red) after $CoCl_2$ treatment,
856 with geneset enrichment analysis revealing several pathways significantly dysregulated after
857 CoCl2 treatment recapitulating changes seen in transcriptomic analysis of late versus early
858 gestation mouse placenta. Scale marker = 200 µm. FCCP= carbonyl cyanide 4-(trifluoromethoxy)
859 phenylhydrazone, an ionophore uncoupler of oxidative phosphorylation which depolarizes mt
860 membrane potential. See Figure 5 - Supplement 3 for assessment of effects of HIF-1
861 stabilization in JAR cells using DMOG. Each data point represents a technical replicate
862 (measurement from an independent well of cells grown in treatment vs control condition). Data
863 normalized to mean of control group. See Fig 5 Source Data 1 for uncropped blots.
864
865 **Figure 5 - Supplement 1.** The mitochondrial effects of HIF-1 stabilization in JAR cells begin to
866 appear on day 3 following $CoCl_2$ exposure. Each data point represents a technical replicate
867 (independent well of cells grown in control vs treatment condition).
868
869 **Figure 5 - Supplement 2**. Increased number of JAR cells stain with propidium iodide, but the
870 absolute number remains low following 6 days of $CoCl_2$ treatment. Each data point represents a
871 technical replicate (independent well of cells grown in control vs treatment condition).
872

873 **Figure 5 - Supplement 3**. DMOG stabilizes HIF-1 in JAR cells (A) and induces similar effects as
874 $CoCl_2$ on COX IV protein (B), SA-βGal expression (C), and cell growth (D) after 4 days. Each data
875 point represents a technical replicate (measurement from an independent well of cells grown in
876 treatment vs control condition). See Figure 5 - Source Data 1 for uncropped blots.
877
878 **Figure 5 - Source Data 1**. Uncropped, unedited blots from 5a (left) and 5c (right)
879
880 **Figure 6. Conditioned media (CM) from JAR cells following HIF-1 stabilization induces**
881 **expression of contractile-associated proteins and augments contraction in immortalized**
882 **human uterine myocytes.** hTERT-HM mRNA expression of *PTGS2* (A), *GJA1* (B), *PTGFR* (C), and
883 *IL6* (D) was induced by CM from JAR cells following $CoCl_2$ treatment (but not in control
884 conditions), potentiating the effect of stimulation of myocytes by exogenous IL-1β. Data
885 normalized to mean of null treatment group. Percent well area occupied by hTERT-HM cells
886 embedded in collagen matrix is significantly smaller after stimulation with IL-1β plus JAR CM
887 from $CoCl_2$ condition, reflecting greater degree of hTERT-HM cellular contraction (E). Each data
888 point represents a technical replicate (measurement from an independent well of cells grown in
889 treatment vs control condition).
890
891 **Figure 7. Maternal DMOG injection on e16.5 stabilizes placental HIF-1 and induces preterm**
892 **labor**. HIF-1α protein is detected in placental lysates 12 hours following DMOG injection but not
893 vehicle (A). mRNA expression of HIF-1 targets *Hk2* and *Slc2a1* is upregulated following DMOG
894 injection ($p = 0.002$ for DMOG vs vehicle, two-way ANOVA) (B). Gestational length is

895 significantly shortened following DMOG injection versus vehicle (C-D). Each data point

896 represents a biological replicate (in A and B, each measurement from an individual placenta

897 collected from one of 2 pregnant dams). Data normalized to mean of vehicle group. See Figure

898 7 - Source Data 1 for uncropped blots.

899

900 **Figure 7 - Source Data 1**. Uncropped, unedited blots from Figure 7.

901

902 **Table 1. Maternal and fetal characteristics**. Data summarized by mean ± SEM or n (%). p-values
903 calculated via t-test (continuous variables) or Chi-square contingency table (categorical
904 variables).
905

		< 35 weeks	> 39 weeks	p value
		n = 9	n = 11	
Gestational age at delivery (weeks)		34.0 ± 0.3	39.5 ± 0.1	< 0.0001
Maternal age (years)		31.9 ± 0.9	36.2 ± 1.0	0.008
Maternal BMI > 40		1 (11)	0 (0)	0.26
Maternal race				
	White	7 (78)	9 (82)	0.13
	Black	2 (22)	0 (0)	
	Asian	0 (0)	2 (18)	
Primiparous		4 (44)	4 (36)	0.71
Female neonate		5 (55)	8 (73)	0.42
Indication for delivery		Placenta previa (3)	Scheduled repeat (7)	
		Vasa previa (4)	Breech presentation (3)	
		Thinned lower uterine segment (2)	Elective (1)	

906
907 Table 2. Primers

908 Mouse

Target	Sequence	Platform

Glb1	Mm00515342_m1	TaqMan
Hk2	Mm00443385_m1	TaqMan
Slc2a1	Mm00441473_m1	TaqMan
D loop (long, 801 bp amplicon)	F: CGTACATTAAACTATTTTCCCCAAG R: GAGTTTTGGTTCACGGAACAT	SYBR
COII/ATPase 6 (long, 855 bp amplicon)	F: TTGGTCTACAAGACGCCACA R: ATTTTGGTGAAGGTGCCAGT	SYBR
Nd5 (long, 930 bp amplicon)	F: CGCCTACTCCTCAGTTAGCC R: ATGGTGACTCAGTGCCAGGT	SYBR
Nd2/Nd1 (long, 832 bp amplicon)	F: GGATGAGCCTCAAACTCCAA R: ATGATGGCAAGGGTGATAGG	SYBR
D loop (short)	F: TGACTATCCCCTTCCCCATT R: TTGTTGGTTTCACGGAGGAT	SYBR
COII/ATPase 6 (short)	F: TCTCCCCTCTCTACGCATTC R: CGGTTAATACGGGGTTGTTG	SYBR
Nd5 (short)	F: GGCCTCACATCATCACTCCT R: GCTGTGGATCCGTTCGTAGT	SYBR
Nd2/Nd1 (short)	F: GGATGAGCCTCAAACTCCAA R: GGCTCGTAAAGCTCCGAATA	SYBR
Actb	Mm00607939_s1	TaqMan

Human

Target	**Sequence**	**Platform**
HK2	Hs00606086_m1	TaqMan
SLC2A1	Hs00892681_m1	TaqMan
IL1A	Hs00174092_m1	TaqMan
IL1B	Hs01555410_m1	TaqMan
TNFA	Hs00174128_m1	TaqMan
IL6	Hs00174131_m1	TaqMan
IL10	Hs00961622_m1	TaqMan
MT-ATP6	Hs02596862_g1	TaqMan
MT-COX2	Hs02596865_g1	TaqMan
ND1	F: CCATAAAACCCGCCACACT	SYBR

	R: GAGCGATGGTGAGAGCTAAGGT	
18S	F: CGCAGCTAGGAATAATGGAATAGG R: CATGGCCTCAGTTCCGAAA	SYBR
GJA1	Hs.PT.58.38338544	SYBR
PTGS2	Hs.PT.58.77266	SYBR
ACTB	Hs.PT.39a.22214847	SYBR
YWHAZ	Hs01122445_g1	TaqMan

911

912 Table 3. Antibodies

Antibody	**Species**	**Working Concentration**	**Source**
CoxIV	Mouse IgG mAb	1:1,000	Cell Signaling Technology, #11967S
β-Actin-HRP conjugate	Rabbit IgG mAb	1:2,000	Cell Signaling Technology, # 5125S
HIF1	Rabbit	1:1000	Cell Signaling Technology, #14179S

913